Industrial Crops & Products 219 (2024) 119018

Contents lists available at ScienceDirect

Industrial Crops & Products

journal homepage: www.elsevier.com/locate/indcrop

Machine learning algorithms to optimize the properties of bio-based poly (butylene succinate-*co*- butylene adipate) nanocomposites with carbon nanotubes

Elizabeth Champa-Bujaico [a], Ana M. Díez-Pascual [b,*], Pilar Garcia-Diaz [a], Valentina Sessini [c], Marta E.G. Mosquera [c]

[a] Universidad de Alcalá, Departamento de Teoría de la Señal y Comunicaciones, Ctra. Madrid, Barcelona Km. 33.6, Alcala de Henares, Madrid 28805, Spain
[b] Universidad de Alcalá, Facultad de Ciencias, Departamento de Química Analítica, Química Física e Ingeniería Química, Ctra. Madrid-Barcelona Km. 33.6, Alcalá de Henares, Madrid 28805, Spain
[c] Universidad de Alcalá, Facultad de Ciencias, Departamento de Química Orgánica y Química Inorgánica, Ctra. Madrid-Barcelona Km. 33.6, Alcalá de Henares, Madrid 28805, Spain

ARTICLE INFO

Keywords:
Machine learning
Carbon nanotubes
Biopolymer
Mechanical properties
Poly[(butylene succinate)-co-adipate]

ABSTRACT

Poly[(butylene succinate)-co-adipate] (PBSA)-based materials are gathering much attention in the packaging industry, agriculture, and other fields owed to their biocompatibility and biodegradability. Nonetheless, poor thermal and mechanical properties of biodegradable polymers, such as PBSA, have hampered their wide-spread use. Herein, a simple, cost-effective and scalable solution to improve the mechanical properties of PBSA is reported by using functionalized single-walled carbon nanotubes (SWCNTs). Different SWCNT loadings have been incorporated in the PBSA matrix via simple solution casting, and the ultrasonication conditions have been optimized to attain a homogenous SWCNT dispersion. The nanocomposites have been characterized in detail by scanning electron microscopy (SEM), Infrared spectroscopy, thermogravimetric analysis (TGA), differential scanning calorimetry (DSC), tensile and impact strength tests. Unprecedented increments in stiffness were found at low nanotube loadings, ascribed to the outstanding reinforcing capability of the SWCNTs combined with their superior modulus and strong interfacial adhesion with the matrix via H-bonding, polar and CH-π interactions. Further, four machine learning (ML) algorithms, Polynomial Regression (PR), Support Vector Machines for Regression (SVR), Gradient Boosting (GB) and Artificial Neural Network (ANN), were applied to predict their mechanical properties. The algorithms performance was assessed using analytical parameters such as the coefficient of determination (R^2), the mean square error (MSE) and the mean absolute error (MAE). The developed models exhibited strong performance, achieving R^2 values ranging from 0.69 to 0.99 across the evaluated properties. The results corroborate that even when the same prediction model is used, its performance varies depending on the physical property to be predicted. Thus, SVR, GB, PR, and ANN were found to be the most effective for estimating the Young's modulus, tensile strength, elongation at break and impact strength, respectively. This research holds great potential for advancing the field of modelling the mechanical properties of polymeric nanocomposites and their practical applications in various industries such as food, pharmaceutical and biomedicine. The development of accurate models for predicting nanocomposite properties would cheapen, simplify and systematize their design and production processes, resulting in improved final products and more efficient development procedures.

1. Introduction

Petroleum resources are limited, hence novel sources of plastics are pursued. The use of biodegradable polymers has environmental advantages such as regeneration of raw materials and reduction of carbon dioxide emissions that led to global warming (Zhu and Wang, 2020). Biodegradable materials can be composted with organic waste or used to generate biomass at their end-of-life. Also, they can be recycled

* Corresponding author.
E-mail address: am.diez@uah.es (A.M. Díez-Pascual).

https://doi.org/10.1016/j.indcrop.2024.119018
Received 9 October 2023; Received in revised form 8 June 2024; Accepted 15 June 2024
Available online 25 June 2024
0926-6690/© 2024 Elsevier B.V. All rights are reserved, including those for text and data mining, AI training, and similar technologies.

to yield monomers and oligomers by microorganisms and used to regenerate the origin products. In the absence of oxygen, anaerobic digestion transforms organic waste into biogas (a mixture of CO_2 and CH_4), which may then be additionally valorized via heat and power (Samir et al., 2022).

Poly[(butylene succinate)-co-adipate] (PBSA) is a biocompatible and totally biodegradable, semicrystalline copolyester produced by condensation of succinic and adipate acid with 1–4-butanediol. Since the Covid-19 pandemic, the request for environmentally friendly bio-based biodegradable materials has raised markedly. In this regard, this aliphatic thermoplastic can now be derived from renewable sources such as sugars (i.e. by means of fermentation of glucose and sucrose) (Platnieks et al., 2021). This biopolymer has adequate mechanical and thermal properties together with good processability via well-stablished techniques such as injection molding, extrusion, solution casting and thermoforming (Xu and Guo, 2010). It displays lower crystallinity and crystallization temperature and it is more flexible than polylactic acid (PLA), hence its processability is simpler, and it straightforwardly degrades in many environments (Lucas et al., 2008). Nonetheless, its properties are influenced by the comonomer ratios, molecular weight and branching. Small molecular weights are desired for extrusion and injection molding, while higher or long branched chains are appropriate for blowing and casting. PBSA can be a cost-effective alternative to other biopolymers such as poly(butylene adipate terephthalate) (PBAT) or polyhydroxyalkanoates such as poly-3-hydroxybutyrate (PHB). It displays a very wide range of potential applications, from food packaging (it meets FDA and European food contact safety standards), textiles, plant pots, hygiene products, and so forth to the electronics and even the locomotive sector as a composite material (Strangis et al., 2023, Koronis et al., 2013). In addition, it can be used in biomedicine for tissue engineering, drug encapsulation and (Brunner et al., 2011) orthopedic applications (Babu et al., 2013) owed to its non cytotoxicity and outstanding biocompatibility (Fukushima et al., 2012). However, the mechanical properties of PBSA do not meet the requirements for certain applications, hence its current use at a commercial scale is limited. In this regard, novel approaches are pursued such as the blending with other polymers (Ojijo et atl., 2012) or the addition of micro/-nanoreinforcements. Thus, a few nanofillers such as silica (Tsimpliaraki et al., 2010), layered double hydroxide (LDH) (Delorme et al., 2022), organic nanoclay and halloysite nanotubes (HNT) (Chiu, 2017), nanocrystalline cellulose (Hosseinipour, et al., 2021) and carbon nanoparticles (Bleija et al., 2022) have been added to this matrix.

Taking into account their excellent physical properties including high stiffness, strength, exceptional electrical and thermal conductivity, low density and very high aspect ratio, carbon nanotubes (CNTs), 1D hollow carbon tubes with a diameter at the nanoscale offer unique possibilities for a wide variety of applications. These include biotechnology, sensors, electronics, and particularly as reinforcement inside a polymer matrix to develop high performance nanocomposites. However, CNTs interact via intermolecular forces named van der Waals forces, and these tube-tube interactions lead to a bundling effect known as clustering or agglomeration that strongly diminishes their physical properties compared with those in a dispersed state. Due to their poor wettability during mixing, CNT- reinforced composites are usually prepared by extrusion, hot pressing, etc. after premixing the matrix and the CNTs powders.

To improve CNT dispersion inside a polymer matrix, CNTs can be functionalized through covalent and non-covalent routes (Díez-Pascual, 2021). The former can be achieved by incorporating chemical functional groups (ie. amine, carboxylic acid, thiol, etc.) on the CNT sidewalls, which is an effective way to improve their dispersibility in aqueous medium. The functional groups on the CNTs can react with functional groups of the polymer to form covalent bonds. Despite covalent functionalization enables a strong interaction between the polymer and the CNTs, it can disturb the π-conjugated system of the nanotubes, hence leading to a lessening in mechanical and electrical properties. Conversely, non-covalent functionalization holds the intrinsic properties of CNTs while imparts novel functionalities. It can be accomplished via π-π interactions (using aromatic compounds or polymers), electrostatic interactions, or CH-π interactions between CNTs and polymers (Tasis et al., 2006), and preserves the biocompatibility of CNTs without impairing their electrical or mechanical characteristics. However, the interaction CNT-polymer is typically weak. In this regard, obtaining homogeneous CNT dispersions in aqueous solutions is still a very challenging task, and novel functionalization approaches are pursued. For instance, a few studies have reported the functionalization of CNTs with poly-3-aminobenzenesulfonic acid (González-Gaitán et al., 2015, Canas et al., 2008), which was beneficial for delivering different properties to the nanotube surface. Furthermore, these modified CNTs were able to polymerize, and the obtained homopolymers displayed improved electrochemical performance.

Artificial Intelligence (AI), that is, the skill of a computer to perform tasks usually linked to human beings, has involved plenty of attention in recent years owed to its huge potential in a wide number of fields (Nilsson, 1997). Two major types of AI have been defined, strong and weak (Scerri and Grech, 2020). The latter focuses on automating specific tasks, while the former is capable of learning and thinking similarly to humans. Machine Learning (ML) is a class of AI that assists computers to reach proper decisions for a given phenomenon based on the processing and knowledge of a large volume of historical data on it. ML includes a group of computer techniques and algorithms designed to perform some type of inference and characterized by their "self-learning" ability, improving the precision of the task progressively, with its execution time. From a collection of input data, algorithms find patterns and relationships between characteristics of the information that they use to make decisions and make predictions about new data. ML is very useful in highly complex problems in which the human mind cannot process enormous amounts of data (big data) or infer complex relationships between them.

Two key types of ML have been identified: supervised learning and unsupervised learning (Mittal and Sharma, 2021). In the first, the input data are labeled, that is, the correct answer that the algorithm should deliver is known (for example, the positive or negative diagnosis of a disease or syndrome). The algorithm "self-learns" to associate characteristics of the input information to solve the labels more accurately. This stage is known as the training and testing step. Once this stage is completed, the algorithm is executed in the evaluation stage with "unknown" data, that is, data for which no previously defined categories or labels exist, and the correct diagnostic output is not offered for each data entry. From the output offered by the tool in this stage, the model performance is estimated in terms of its accuracy at predicting on unseen data samples. Supervised learning is designed for regression and classification tasks; for example, from biomarker values of a certain disease of a set of individuals, the algorithm predicts whether or not they suffer from the pathology studied. It is evident that larger data sets during training will provide greater accuracy in decisions with new data from unknown labels. To ensure satisfactory performance, it is very important to guarantee the use of unbiased data for training.

In unsupervised learning, the training data are not labeled, so the algorithm is unaware of the correct output or result that it should provide even in the training stage. The algorithm extracts features such as patterns and relationships in the data it modifies by comparing the predicted and actual label, when provided a posteriori. It must be provided with large amounts of data to allow it to "self-learn" and progressively enhance accuracy. A commonly used unsupervised learning technique is clustering by classes or categories, in which highly complex data can be organized into similar groups to extrapolate algorithmic relationships.

In material science, ML can be used at several stages, from material design to property prediction. It promotes the speed up of the research and development process, and contributes to get knowledge and to the optimization of properties and processes related to different types of

materials, including polymers and their composites (Wang et al., 2020). In particular, ML demonstrates countless potential to predict the properties of polymeric nanocomposites based on their composition and structure (Champa-Bujaico et al., 2022). These composites comprise a continuous matrix phase and a dispersed nanoreinforcement phase. The matrix allocates the load across the whole surface area of the reinforcement phase. Several factors condition the effectivity of the nanofiller phase as reinforcement, including its nature and type, concentration, aspect ratio, shape, size, orientation, and dispersion within the matrix. In this regard, 3 different morphologies have been described: separated, intercalated, and exfoliated.An intercalated morphology is formed if the polymeric chains are inserted among the nanofillers, whereas an exfoliated morphology appears when the nanofiller is uniformly and thoroughly dispersed through the continuous polymer matrix. One of the most important characteristics of polymer nanocomposites is their potential to show improved properties upon addition of very small amounts of the nanoreinforcement, since the final thermal and mechanical properties are directly related to the developed morphologies. Further, they typically display synergic effects, and the final composite properties surpasses the sum of the individual components.

The synthesis process of the nanocomposites also influences strongly their mechanical behaviour. Polymer nanocomposites are typically prepared via melt-blending, compression moulding, solution processing and in-situ polymerization. Further, their mechanical performance is influenced by other factors, including residual stress and strain. In particular, the stiffness and toughness of the nanocomposites depends on the stress transfer ability from the matrix to the nanoreinforcement phase, which have different elastic moduli and Poisson's ratios. An overview of current advances on the application of (ML)-driven approaches for the logical design of polymer nanocomposites has been recently reported (Saxena et al., 2023). ML algorithms are trained from a vast amount of data and stablish correlations between input fingerprints and output attributes, leading to an accurate prediction of the nanocomposite properties (i.e. mechanical, thermal, optical, electrical). By minimizing the need for extensive testing or computationally challenging developments of extensive models, ML offers a precise analysis of the behavior of the nanocomposites.

Numerous models including Multiple Linear Regression (MLR), Artificial Neural Networks (ANNs), Random Forest (RF), Decision Tree (DT) Support Vector Machines (SVMs), Bayesian learning, Gradient Boosting (GB), K-Nearest-Neighbor (KNN), Gaussian Process Regression (GPR), to mention just some examples, have been applied to predict the properties of polymeric materials (Bock et al., 2019) (Maulud, 2020) (Huang, 2020). For instance, ANN, RF, and MLR have been used to predict the mechanical properties of ternary nanocomposite films comprising polyvinyl alcohol (PVA), oxidized cellulose nanofibers and either ammonium zirconium carbonate or glyoxal, and it was found that ANN lead to the best performance while MLR had the lowest accuracy (Cencer et al., 2022). Similarly, the properties of multiscale polyhydroxyalkanoate/graphene oxide/nanoclay bionanocomposites were optimized by ANN, DT and SVM, and the results demonstrated that ANN and SVM are useful for estimating the Young's modulus and elongation at break, while DT was more suitable for predicting the tensile strength (Özkan et al., 2019). Gaussian Process Regression (GPR) model was applied to predict the tensile strength of carbon nanotube reinforced polymeric matrices, and very good correlations were obtained (Le, 2021). The mechanical properties of high-density polyethylene (HDPE)/nanodiamond nanocomposites have also been assessed using ANN, and very accurate predictions were obtained for the Young's modulus and hardness of the nanocomposites (Sahu and Sreekanth, 2022). The abovementioned studies suggest that ML methods can be effective in predicting the mechanical properties of nanocomposites. However, studies on this topic are still very scarce, and to the best of our knowledge, no previous work on the prediction of the mechanical properties of composites based on a biopolymer matrix such as PBSA has been reported to date.

PBSA matrix was chosen in this work as a promising bio-based, biodegradable and environmentally sustainable polymer matrix for use as an alternative to commodity plastics in food packaging, medicine as drug transport materials, medical implants, wound healing, tissue scaffolds and in the pharmaceutical industry. It has been reinforced for the first time with different amounts of CNTs via an easy and inexpensive solution casting method to enhance the mechanical properties. By tuning the carbon nanotube loading and the processing parameters (sonication time and amplitude), the stiffness and strength can be carefully tailored to attain specific requirements for targeted applications. Further, different ML-based algorithms (PR, SVR, GB and ANN) have been applied to predict their mechanical properties. The characteristics of each model are detailed in the following section. The minimum squared errors (MSE), mean absolute errors (MAE) and coefficient of determination (R^2) have been compared to find out the best model for each mechanical property. The proper connection between ML algorithms and the design of polymer composites is crucial for innovative and novel material manufacturing.

2. Machine learning algorithms

In this study, five types of regression models were initially selected to predict the mechanical properties of the hybrid nanocomposites: Polynomial Regression (PR), Support Vector Regression (SVR), Gradient Boosting (GB), K-Nearest Neighbours (KNN) and Artificial Neural Networks (ANN). The main characteristics of each model are detailed below. The main reason for the selection of the four machine learning algorithms was their high acceptance in the specialized literature in this area. The PR, SVR, GB and ANN are very frequently used for predicting mechanical and electrical properties of polymeric materials, among which the ANNs are clearly at the cutting edge. Other ones could have been utilized such as Gradient Descent, Logistic Regression, Bayesian Learning, K Nearest Neighbor, Decision Tree, Genetic Algorithm, PSO, Harmony Search, and so on (Bock et al., 2019) (Maulud, 2020). However, SVM and ANN generally outperform the above both in accuracy and prevalence of use (Huang, 2020).

2.1. Polynomial regression

PR is used in statistics and ML to correlate variables that do not follow a linear pattern (Ostertagová, 2012). Unlike linear regression, which fits a straight line, polynomial regression employs a higher degree polynomial in order to capture complex patterns existing in the data more effectively. This method is particularly useful when the data show a curvilinear trend (Heiberger and Neuwirth, 2009), and cannot be adequately modelled by a linear equation. The goal of PR is to find the polynomial function of degree n that best fits the input and output data. The general expression for a polynomial of degree n is:

$$y=\beta_0+\beta_1\boxdot x+\beta_2\boxdot x^2+\ldots+\beta n\boxdot x^n$$

(Heiberger and Neuwirth, 2009)

where y is the output variable being predicted, x, is the input variable, n, is the degree of the polynomial and β_0, $\beta_1 \ldots \beta_n$ are the coefficients that are fitted during the regression process.

2.2. Support Vector Regression

SVR is a technique in which hyperplanes are defined to distinct or discern categories in the input data. It is a type of support vector machine (SVM), a supervised ML algorithm that can be used to solve both classification and regression problems (Maimon, 2010). In the context of regression, SVR is used, and the main goal is to find a function that fits the data optimally (Li et al., 2009). This function seeks to minimize the differences between the predictions made by the model and the real values of the training data. Simultaneously, SVR takes into account the simplicity of the model, striking a balance between the fit to the data and

the complexity of the model (Friedman et al., 2001, Cristianini and Shawe-Taylor, 2002).

Several parameters can be tuned to obtain an optimal regression model: A) The cost factor, C, which governs the trade-off between the fit to the training data and the generalisability of the regression model. B) The Kernel type, which fixes how the data are transformed into a higher dimensional feature space. Different kernel types, such as linear, polynomial or radial (RBF) can be chosen (Li et al.,2009). Herein, the RBF kernel function was used, which is highly valuable for managing non-linear relationships in regression (Guenther and Schonlau, 2016). C) Gamma parameter, which determines the effect of neighboring data points on predictions. D) Epsilon parameter, which sets the tolerance range for prediction errors. It specifies how much predictions are allowed to diverge from the true values within a defined range (Hsu and Lin, 2002).

2.3. Boosting

Boosting is an ensemble learning technique that seeks to enhance the performance of simpler (Schapire, 2003), less effective models by transforming them into more robust and accurate versions that can more effectively generalise the data (Freund and Schapire, 1999; Várkonyi-Kóczy, 2020). At each algorithm step, a weak model is trained using the dataset and the weights of the training instances are adjusted to give more weight to those that were erroneously predicted in previous steps. Then, a new weak model is trained considering these updated weights. This process is repeated several times and the resulting weak models are combined in a weighted way to form a final model, often leading to a significant improvement in model accuracy and performance. There are several boosting algorithms, such as AdaBoost, Gradient Boosting (GB) and XGBoost. GB was used herein, which is a boosting algorithm that commonly works by building decision trees at each iteration and combining them to create a stronger model (Aler et al., 2017). The number of trees used is called the number of weak estimators. The characteristic parameters of this algorithm are the learning rate, which adjusts the contribution of each tree to the final prediction, and the maximum tree depth, which limits the complexity of the trees.

2.4. K- nearest neighbours

KNN is a versatile technique used to classify data or perform regressions (Bafandeh Imandoust and Bolandraftar, 2013). It works by evaluating the similarity between data points in a feature space (Kramer, 2013). The distance between a new point and all training points (data) is calculated by identifying the K closest points. In the case of regression, this methodology allows predicting values based on their proximity to existing data (Heiberger and Neuwirth, 2009). When K is set to 1, the "Nearest Neighbour" (1-NN) approach is adopted (Biau and Devroye, 2010). In this configuration, the prediction is based solely on the value of the nearest point in the training data set, which makes it possible to effectively capture non-linear relationships in the data (Guégan and Huck, 2005). This approach can result in predictions sensitive to outliers but offers flexibility and simplicity in predictive decision making.

2.5. Artificial neural network

ANN are computational models inspired by the architecture and operations of the human brain with the objective of uncovering and understanding the fundamental relationships within a given dataset (Anifowose and Eludiora, 2002). A set of interconnected nodes, called artificial neurons, are built, and organized into layers that process information. Layers are structured in three types: the input layer, the output layer and one or more hidden layers. Neurons are characterized by an activation function that contributes to the non-linearity into the model. Neurons in the input layer receive input data, those in the hidden layers perform computations and transformations, and those in the output layer generate the final outputs of the network (Drew and Monson, 2000, Zou et al., 2008). Neurons are linked via weighted connections, which establish the relative relevance of the associated input in the calculation of a unit output. These weights are tuned throughout the training process to improve the performance and predictions of the neural network (Zou et al., 2008, Levy Mangin et al., 2008).

The fundamental configuration of a neural network may change depending on the nature of the problem and the architecture employed (Abraham, 2005). Among the most frequent structures are: a) Perceptron, which consists of a single hidden layer of units, where each neuron is connected to the input layer and produces an output based on an activation function. It is suitable for linearly separable binary classification problems (Rosenblatt, 1962). b) Feedforward Neural Networks, also referred to as multilayer neural networks. These are systems in which information flows in a unidirectional manner from the input layer to the output layer, without cycles or feedback loops. They are well-suited for tackling complex classification and regression problems and have the capability to learn feature representations. c) Convolutional neural networks (CNN), are frequently used in image recognition problems since they can work with a very large dataset, performing a dimensionality reduction (Lo et al., 1995). d) Recurrent Neural Networks (RNNs), are able to maintain and use previous information in their operation, either by feeding back their own outputs or by connecting to previous layers. This makes them especially useful for working with data that have a sequential or temporal structure, such as text and audio (Mandic and Chambers, 2001).

In this study, input data representing the chemical composition of the polymer nanocomposites, and output data corresponding to the specific experimental mechanical properties (Young's modulus, tensile strength, strain at break and impact stress) have been used. Different ANNs have been compared with each other to assess the most accurate in predicting the properties of the materials under study: gradient descent and the Gauss-Newton method together with the Levenberg algorithm (Gavin, 2023, Hagan and Menhaj, (1994)). The Feedforward neural network architecture was used. It has an input layer with one neuron representing each different chemical property of the nanocomposite, one or more hidden layers in the middle, depending on the problem to be solved, and an output layer with a single neuron that provides the final prediction. The hidden layers use a mathematical function known as ReLU, which aids the network to learn non-linear patterns in the data (Berner et al., 2019). A learning rate of 0.008 for ANN-LV and a maximum number of iterations of 1000 have been set as initial parameters of the training algorithm. These values can be tailored according to the problem and the network architecture. The maximum number of iterations has been set to avoid model over-fitting and to control the length of the training process. It is imperative to correctly tune the model parameters, which may require a trial-and-error approach for each specific problem. Herein, the data have been split into two groups: one to train the model and one to evaluate it and measure its accuracy. The ANN has been built with the TensorFlow functional API tool, which is widely used to develop ML models for complex regression problems. This model has been developed in Python version 3.9.6 using the Keras version 2.10.0 and TensorFlow version 2.10.0 libraries. These libraries are open-source and can be used for free.

The quality of the developed models was assessed by determining the mean absolute error (MAE), the mean square error (MSE) and the coefficient of determination (R^2). MSE is calculated as the mean of the squares of the differences between the predicted and the experimental values. It is defined as follows:

$$MSE = \frac{1}{n}\sum(y' - y)^2$$

where y' is the predicted value, y is the corresponding value and n is the

total number of samples in the data set.

MAE is calculated as the average of the absolute differences between the predicted and experimental values:

$$MAE = \frac{1}{n}\sum|y' - y|$$

MAE is less sensitive to outliers than MSE as it uses absolute values instead of squares. Though, by not squaring errors, MAE may underestimate the impact of big errors.

R^2 is the fraction of the variation in the dependent variable that is predictable from the independent variable(s), and is calculated as:

$$R^2 = \left(\frac{n(\sum yy') - (\sum y)(\sum y')}{\sqrt{[n\sum y^2 - (\sum y)^2][n\sum y'^2 - (\sum y')^2]}}\right)^2$$

R^2 is commonly used to assess the accuracy of ML models. It is a measure of the goodness of fit, and indicates the degree of correlation between the model prediction and the target values. The closer the R^2 is to 1.0, the better the accuracy of the model is.

3. Materials and instruments

Bio-based poly(butylene succinate-co-butylene adipate) (PBSA), FD92PM grade, was purchased in pellet form from PTT MCC Biochem Company Ltd. (Bangkok, Thailand). According to the manufacturer, this grade is suitable for blown film applications, i.e., bag liners, mulch films, agricultural films, and it is a food contact grade that complies with the EU10/2011 standard. It is compostable and biodegradable, and can be processed via extrusion, injection moulding and film casting. Its properties are: d25°C = 1.24 g/cm3, MFR (190°C, 2.16 kg) = 4 g/10 min, and Tm = 84°C. According to Gel Permeation Chromatography (GPC), the polymer has a number average molecular weight Mn of 45369 g/mol and a weight average molecular weight Mw of 116237 g/mol. Polyaminobenzenesulfonic acid functionalized single-walled carbon nanotubes were provided by Sigma Aldrich (Madrid, Spain). Their outer average diameter was 1.1 nm, and their length ranged between 0.5–1 μm, with a purity of 85 %. Dichloromethane (DCM, CH2Cl2) was also provided by Sigma-Aldrich. All the reagents were used as received. The chemical structure of PBSA and the polyaminobenzenesulfonic acid functionalized CNTs is shown in Scheme 1. To simplify the nomenclature throughout the work, the carbon nanotubes will be designated just as SWCNTs.

Probe sonication was carried out with a Vibra-Cell 75042 ultrasonic processor (Bioblock Scientific, Madrid, Spain) incorporating a titanium probe of 15 mm diameter, operating at 220 V, 20 A, 60 Hz, and single phase. A Kern ABT 150–50 M analytical balance (precision ± 0.01 mg) was used to weight the nanocomposite components.

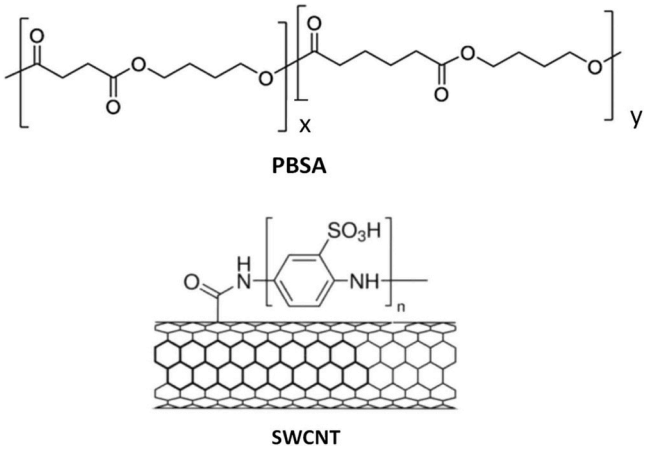

Scheme 1. Chemical structure of poly(butylene succinate-co-butylene adipate) (PBSA) and polyaminobenzenesulfonic acid functionalized single-walled carbon nanotubes (SWCNTs).

3.1. Preparation of PBSA/SWCNT nanocomposites

The nanocomposites were prepared via simple ultrasonication followed by solution casting technique. In short, PBSA pellets were weighed and completely dissolved in DCM at RT, followed by addition of the required amount of the functionalized SWCNTs under continuous stirring. Each mixture was then ultrasonicated to attain a uniform dispersion of the SWCNTs in the solution. Different ultrasonication times (1, 2, 3, 4, and 5 min) and amplitudes (70, 75, 80, 85 and 90 %) were tested in order to select the optimal conditions. Each nanocomposite mixture was then stirred for 3 h at RT, enabling a strong interaction between the matrix and nanofiller phases, and finally cast onto a glass Petri dish followed by drying in a vacuum oven to ensure a complete evaporation of the solvent. Nanocomposite films with SWCNT loadings in the range of 0.15–1.0 wt% were prepared. Higher loadings were also tested but resulted in poorer performance.

3.2. Characterization techniques

The fracture surface morphology of the nanocomposites was inspected by scanning electron microscopy (SEM) using a scanning electron microscope (Zeiss, SIGMA VP-500, Germany), operating at an acceleration voltage of 25 kV and different magnifications. The samples were first cryo-fractured and then sputtered with a gold layer under vacuum to prevent charging during electron irradiation.

Gel permeation chromatography (GPC) was carried out on an Agilent 1260 Infinity II high-speed liquid chromatograph to determine polymer weight-average molecular weight (M_w), number-average molecular weight (M_n) and dispersity indexes ($Đ = M_w/M_n$). The analysis of the samples (1 mg ML^{-1} in THF) was performed at 35 °C using tetrahydrofuran as the eluent at a flow rate of 1.0 ML min^{-1} in two Mixed D columns connected in series. Calibrations were performed using polystyrene standards.

The attenuated total reflectance (ATR) FT-IR spectra were acquired on a Spectrum One spectrometer (PerkinElmer, USA) equipped with a Universal ATR sampling accessory (diamond crystal) and a red laser excitation source (632.8 nm), at 25°C, in the wavenumber range between 4000 and 400 cm^{-1}.

The thermal stability of the nanocomposites was studied by thermogravimetric analysis (TGA) using a TGA55 analyzer (TA Instrument, USA). Dynamic experiments were performed on samples of about 10 mg under a nitrogen atmosphere with a gas flow of 60 ML/min. Samples were heated from room temperature to 600 °C at a rate of 10 °C/min. The initial degradation temperatures (Tonset and T5 %) were determined at 2 and 5 % mass loss, respectively, while the temperature at the maximum degradation rate (Tmax) was calculated from the first derivative of the TGA curves (DTG).

DSC measurements were performed with a Q2000 differential scanning calorimeter (TA Instruments, USA) under a nitrogen flow of 50 ML/min. Samples of about 2–3 mg were placed in hermetic Al pans with lids and heated from −90–140°C, cooled down and then heated again, all the stages at a rate of 10°C/min. The degree of crystallinity (Xc) for the neat polymer and the nanocomposites was calculated using the following equation:

$$Xc = \Delta Hm/\Delta Hm0(1 - Wf) \times 100\% \quad (1)$$

where ΔHm is the measured crystallization enthalpy of each sample, ΔHm0 is the enthalpy of a 100 % crystalline polymer (142 J/g for 100 % crystalline PBSA (Pradeep et al., 2017)) and Wf is the weight fraction of the SWCNTs in the nanocomposite.

Tensile tests were carried out following the ASTM D 638–03 standard on a servo-hydraulic testing machine (858 Mini Bionix, MTS Systems

Corporation, MN, US) at a crosshead speed of 1 mm/min and a load cell of 100 kN, under 23°C and 50 % RH. All the samples were conditioned for at least one day before the measurements. Impact strength tests were carried out according to the ASTM D 6110–10 standard under the same environmental conditions using a drop weight impact testing machine (Instron, MA, US). To check for repeatability, five specimens for each type of nanocomposite were tested, and the average value is reported.

3.3. Machine learning model system

The database used was composed of 211 experimental measurements with a percentage of SWCNT between 1 and 10 wt%, which included the experimental measurements of the parameters that characterize the mechanical properties: Young's modulus, tensile strength, elongation at break and impact strength. From the overall samples, 16 were removed since they did not contain all four measurements. Finally, we worked with 195 samples, on which cross-validation was applied to generate the training and evaluation datasets in a proportion of 85–15 %, respectively.

It was not required to apply any preprocessing action on the input data, since the ML algorithms work directly with the composition of the nanocomposite in the polymeric material. Interpolation was also not performed to determine incomplete data values; instead, we chose to remove incomplete experimental data.

The representativity of the data set used is the ML algorithms is based on their suitability to represent an enough size of experimental measurements, to train and evaluate the models by covering an interval with a sufficient interest degree in the presence of nanocomposites in the composition of the polymeric material. This allows us to consider that the input information contains the relevant relationships in the input-output function of the learning models.

Fig. 1 shows a scheme of the ML process. The input data correspond to the 195 real samples of the PBSA with different concentrations of SWCNT on which the experimental measurements have been performed: Young's modulus, tensile strength, elongation at break and impact strength. To avoid overfitting, cross validation is applied by generating N random training and evaluation sets. The training and test subsets in each pair i are disjoint. The size of the training sets is 85 % of the input set (166 items). The evaluation sets contain the remaining 15 % (29 items).

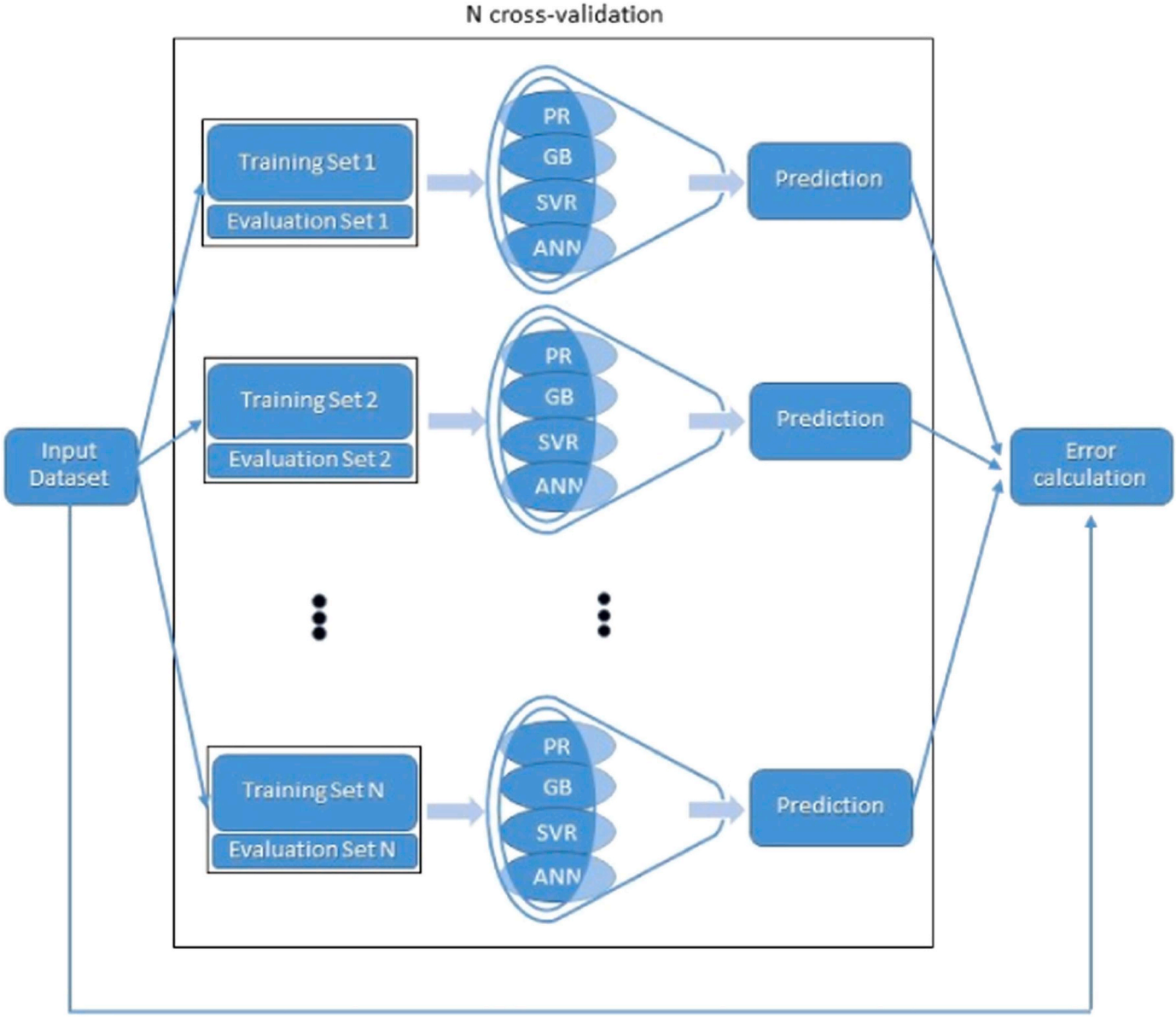

Fig. 1. Schematic representation of the machine learning process applied in this work.

ML models are applied on each pair of *i* data sets. First, the models train with the training subset, but they do not know the values of the evaluation one. This means that they do not know the values of the Young's modulus, tensile strength, elongation at break and impact strength of the evaluation subsets. After training the models, they are applied to the evaluation data. The models provide their predictions of the mechanical properties from the evaluation data. The prediction error is calculated from the experimental values of the mechanical properties and the predicted values.

4. Results and discussion

4.1. Surface morphology of PBSA/SWCNT nanocomposites

A homogeneous SWCNT dispersion within the matrix phase is crucial to design nanocomposites with enhanced thermal and mechanical properties. This is commonly a difficult task, because carbon nanotubes have strong tendency to join together and form bundles. To assess the state of nanofiller dispersion and the morphology of the fabricated composites, the surfaces of cryofractured films were observed by SEM. Typical images of nanocomposites with different SWCNT loadings prepared via ultrasonication for 5 min at an amplitude of 85 % are shown in Fig. 2. These conditions were selected as optimal based on the results of the mechanical tests, as will be discussed later.

In the samples with low nanofiller concentration (0.25 and 0.5 wt%, Fig. 2a and b), the functionalized SWCNTs appear as white spots or curled ropes corresponding to small nanotube bundles, with diameters in the range of 10–22 nm that are homogeneously and randomly distributed within the polymer matrix. No SWCNT agglomerations or entanglements were observed in the scanned areas; the energy of the ultrasonication process breaks up the aggregates, resulting in a fine dispersion of the SWCNTs, which results in a large nanotube-matrix effective contact area. Moreover, no open holes or voids were detected around the SWCNTs, pointing towards a strong matrix-filler interfacial adhesion. This enhanced interaction is ascribed to the incorporation of the functionalized nanotubes, that can interact with the ester groups of the matrix via hydrogen bond formation with their hydroxyl and amino groups of the aminobenzenesulfonic moieties. Further, polar interactions can also take place between these groups, strengthening the interaction.

Conversely, in the images of nanocomposites with higher nanofiller concentration (0.75 and 1 wt%, Fig. 2c and d), the nanotubes are not uniformly distributed but tend to concentrate in certain regions of the matrix, forming a highly entangled interconnected structure. They appear quite agglomerated, particularly in the sample with the highest loading, in which clear aggregates were detected. They show average bundle diameters in the range of 20–35 nm, and length up to 1 μm. It is worthy to note that the trend observed with the SWCNT concentration described above was similar for the different ultrasonication times and amplitudes tested, that is, increase in the formation of aggregates upon increasing SWCNT concentration. Further, for low ultrasonication times (i.e., 1 or 2 min) or low ultrasonication amplitudes (70 or 75 %), some aggregates were detected for almost all the concentrations tested, indicating that such conditions are not effective enough to yield a homogeneous nanotube dispersion within the matrix.

Overall, SEM observations ratify the satisfactory dispersion of the SWCNTs in the nanocomposites with low nanofiller loading, ascribed to the combination of an effective mixing stage under ultrasonication and the functionalization of the SWCNTs, that promotes their interaction with the matrix. The SWCNTs were debundled and split into small ropes by the disentanglement process in the ultrasonic probe, corroborating the efficiency of this mechanochemical pretreatment.

4.2. IR spectrum of PBSA/SWCNT nanocomposites

The FTIR spectrum of neat PBSA and the nanocomposites were recorded to get information about the SWCNT–matrix interactions, and characteristic spectra of nanocomposites prepared via ultrasonication for 5 min at an amplitude of 85 % are shown in Fig. 3. In the spectrum of raw PBSA, the band in the range of 3000−2800 cm^{-1} is ascribed to the C-H asymmetric stretching, and the corresponding symmetrical vibration appears at 1340 cm^{-1}. A very strong band is found at 1725 cm^{-1} arising from the C═O stretching of the ester group. Previous studies reported that these peaks arise from the overlapping of the carbonyl stretching of the amorphous and crystalline regions of the semi-crystalline polymer (Mallardo et al., 2016). The peaks in the range of

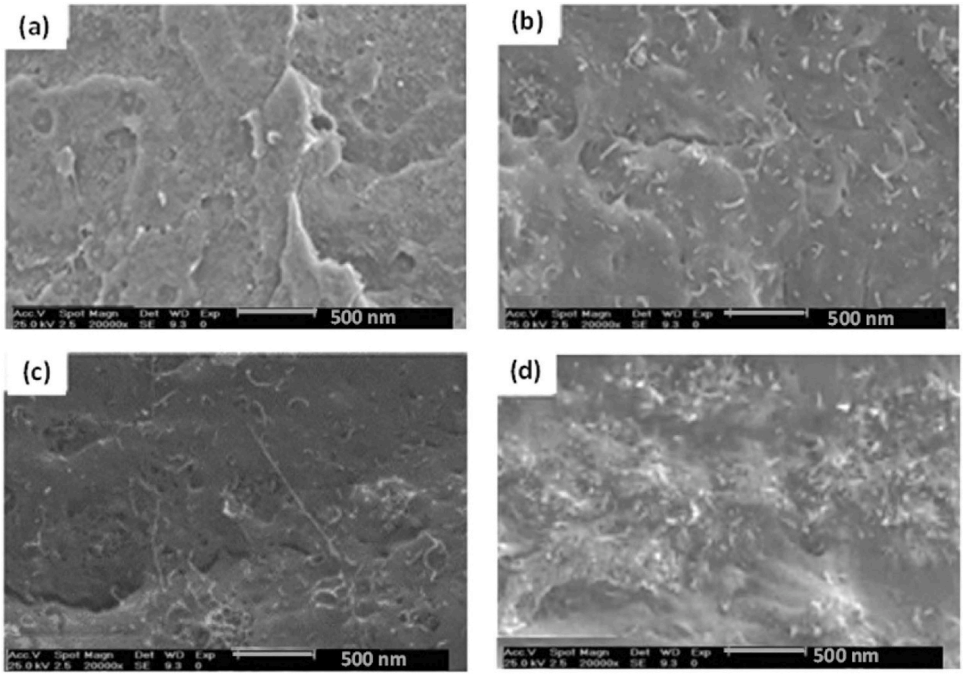

Fig. 2. SEM images from fractured surfaces of PBSA/SWCNT nanocomposites with different SWCNT loadings: a) 0.25 wt%; b) 0.5 wt%; c) 0.75 wt%; d) 1.0 wt%, prepared via ultrasonication for 5 min at an amplitude of 85 %.

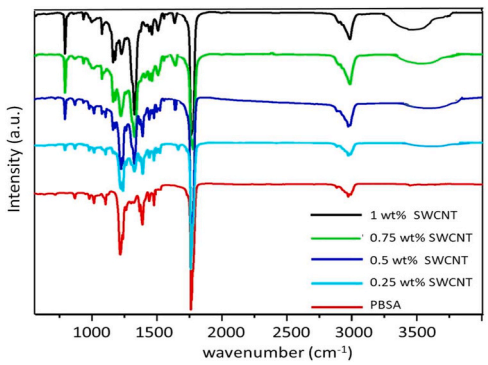

Fig. 3. FTIR spectra of neat PBSA and the nanocomposites prepared via ultrasonication for 5 min at an amplitude of 85 %, with different SWCNT loadings.

1150–1300 cm^{-1} correspond to the –C–O–C– stretching of the ester bonds, and the band at about 1050 cm^{-1} is attributed to the –O–C–C– stretching vibration. Further, the peak at around 950 cm^{-1} is related to the –C–OH bending (Hexig and Hexig, 2012).

Some additional bands can be observed in the spectra of the nanocomposites, that show increased intensity with increasing SWCNT loading, thus corroborating the presence of the nanotubes. A broad band is observed in the range of 3400–3700 cm^{-1} related to the N-H stretching of the amino groups and the O-H stretching of the sulphonic acid moiety of the carbon nanotubes. Further, this band shifts gradually towards lower wavenumber with increasing SWCNT loading, indicative of the formation of hydrogen bonds with the ester groups of the matrix. Thus, it has been reported that the interactions between functionalized SWCNTs and polyesters lead to a broadening of the N-H or O-H stretching band and cause a small downshift (Antolin-Ceron, 2023). Conversely, the band related to the C═O stretching shows a small upshift, as reported earlier for hydrogen acceptors (Joseph and Jemmis, 2007). Further, the slight change in the position of this band could also be related to the change in crystallinity upon addition of the SWCNTs, as will be discussed in the following section, since its shape and position depend on the fraction of amorphous and crystalline regions (Chen et al., 2023). Moreover, the band related to the C-H stretching shifts towards higher wavenumber upon increasing SWCNT loading, indicative of the existence of CH-π interactions between the CH_2 groups on PBSA chains and the sp^2 aromatic structures of the CNTs, in agreement with results reported earlier for nanocomposites reinforced with carbon nanofibers (Song et al., 2015).

On the other hand, new peaks appear at 1580 cm^{-1}, related to the C-C stretching of the main structure of the SWCNTs, at about 1400 cm^{-1} related to the S═O stretching of the sulfonic acid, at 1240 cm^{-1} related to the amide III band, arising from N-H in-plane bending coupled with C-N stretching vibrations (Ji et al., 2020), and at 1080 cm^{-1} related to the O-H in plane bending. All the abovementioned facts corroborate the presence of the SWCNTs in the nanocomposites and the strong nanofiller-matrix interactions, that strengthen on increasing nanotube loading.

4.3. Thermal stability

One of the main weaknesses of copolyesters is their low thermal stability, since thermal degradation can take place during processing. Thus, it is imperative to investigate the effect of the SWCNTs on the decomposition of this copolymer. Fig. 4 shows the TGA and the derivative (DTG) curves of neat PBSA and its nanocomposites with increasing SWCNT loadings. Degradation of all the samples occurred in a single major weight loss step. All the nanocomposites showed an initial degradation temperature (Tonset) and a temperature of 5 wt% weight loss (T5 %) close to those of neat PBSA (295 and 316ºC, respectively, see Table 1). A very slight increase in these temperatures is in general observed for the nanocomposites with higher SWCNT concentrations. Further, they also exhibit a temperature of maximum rate of weight loss (Tmax) close to that of neat PBSA, 382ºC, albeit slightly reduced, particularly for the nanocomposites with low SWCNT contents (Table 1).

Table 1
TGA parameters for neat PBSA and nanocomposites with different SWCNT loading prepared via ultrasonication for 5 min at an amplitude of 85 %. Tonset: initial degradation temperature at 2 % weight loss; T5 %: temperature at 5 % weight loss; Tmax: temperature of maximum rate of degradation; R500: residue at 500ºC.

SWCNT (wt%)	T_{onset} (°C)	$T_{5\,\%}$ (°C)	T_{max} (°C)	R_{500} (%)
0	295.3	316.2	382.4	0.22
0.15	298.5	317.5	378.3	1.28
0.25	297.2	318.7	375.5	1.54
0.50	295.9	316.7	379.3	2.04
0.65	299.7	319.8	380.9	2.26
0.75	292.6	314.6	382.6	2.43
0.85	286.7	313.7	379.5	2.56
1.0	296.6	319.4	381.6	2.89

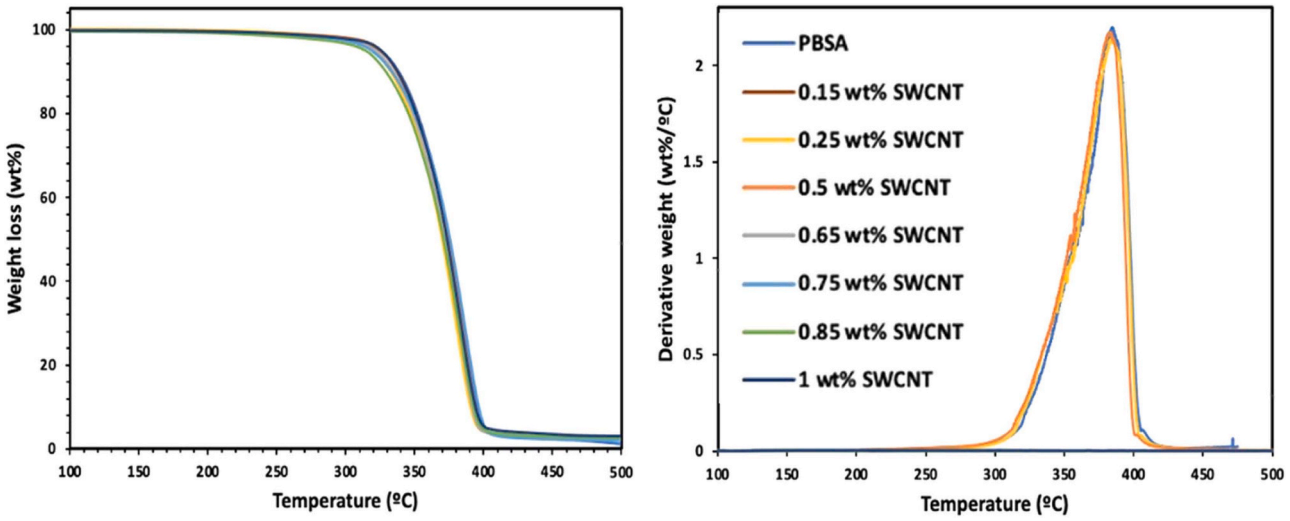

Fig. 4. TGA (left) and DTG (right) thermograms of neat PBSA and nanocomposites with different SWCNT loadings.

Though, the differences observed are quite small, thus results indicate no significant change in the thermal stability of PBSA when the SWCNTs are incorporated to the polymeric matrix, as reported earlier for other nanofillers (Seggiani et al., 2021).

According to the mechanism proposed by Buxbaum for polyesters, the degradation is due to a random cleavage of the ester bond that takes place owing to the β-CH hydrogen transfer. This chain scission results in the formation of oligomers with carboxylic end groups and vinyl groups (Buxbaum, 1968), and the rate of chain breakage increases significantly upon rising temperature, finally leading to the formation of acetaldehyde. Thermal stability enhancement of semicrystalline polyesters has been attained via hydrogen bonding (Hayashi and Tournilhac, 2017) since it hinders the homolytic chain scission. Thus, on the one hand, it would be expected that the SWCNTs will increase the thermal stability of the matrix, since the formation of hydrogen bonds with the matrix would lead to a physical crosslinked network that would degrade at a slower rate. Besides, the free volumes between polymer chains are occupied by carbon nanotubes; therefore, chains are much more squeezed and crosslinking density increases. The increased interfacial interaction between the SWCNTs and PBSA would lead to an increase in the degradation activation energy. Additionally, the nanofillers can act as barriers, restraining the release of volatile products at the polymer degradation, which would be reflected in higher thermal stability. Further, CNTs could form a conductive network facilitating the phonon transfer, leading to high thermal conductivity, which can lighten the local overheating and improve the thermal stability of the nanocomposites (Imran et al., 2022).

Conversely, it has been reported that functionalized carbon nanotubes can lead to a reduction in the thermal stability of the matrix due to a reduction in thermal diffusivity. In particular, it was found that nanotubes modified with amino groups, though they lead to an increase of epoxy matrix crosslinking density, result in faster degradation of the matrix, and the decomposition temperature decreased with increasing the CNT weight fraction (Ciecierska et al., 2013). Similar results were reported for other polymeric matrices reinforced with functionalized SWCNTs (Bozeya et al., 2012, Rodrigues et al., 2021). The addition of the nanotubes improved the mechanical performance while reduced slightly the thermal stability. Further, carbon nanotubes used for this work have 85 % purity, which means that 15 % corresponds to impurities in the form of amorphous carbon and residual metal catalysts. It has been reported (Li et al., 2012) that these impurities or the presence of defects such as acid functional groups on the CNT sidewalls can lead to a decrease in thermal stability of the nanocomposites by the reduction of the scavenging capabilities of free radicals.

On the whole, the thermal conductivity, the effect of scavenging free radicals of CNTs, their percentage of defects and impurities, their size, possibility of hydrogen bonding formation, etc. to mention but a few are factors that came into play in the thermal decomposition mechanism, and the overall result found herein is that the thermal stability is preserved.

4.4. DSC analysis

Differential scanning calorimetry tests were performed to evaluate and compare the effect of the reinforcement addition on the melting and crystallization temperature of PBSA, and typical DSC thermograms of the first cooling and second heating are shown in Fig. 5. The glass transition, melting and crystallization temperatures and the degree of crystallinity of the samples are collected in Table 2.

A well-known characteristic of amorphous and semi-crystalline polymers is to exhibit a second-order transition named as glass transition, wherein the polymer changes from glassy to rubber-like behaviour. Accordingly, the factors that affect chain mobility, ie. crosslinking, crystallinity, and presence of nanofillers would affect the Tg. It would be expected that higher levels of cross-linking, crystallinity, or nanofiller loadings result in higher Tg values. However, results obtained herein

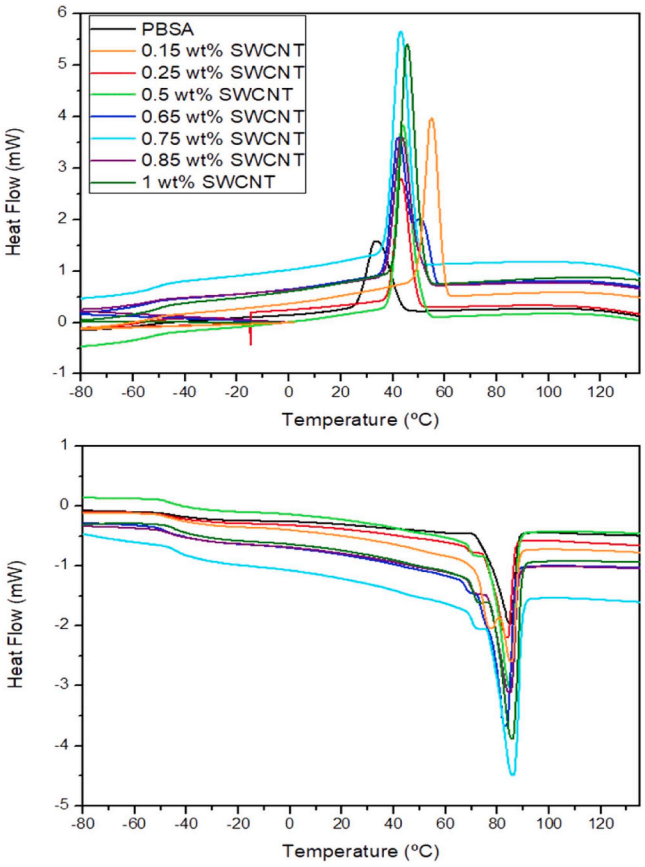

Fig. 5. DSC cooling (exo, top) and heating (endo, down) thermograms of neat PBSA and the nanocomposites with different SWCNT content.

Table 2
DSC parameters for neat PBSA and the nanocomposites. Tg: glass transition temperature Tm: melting temperature; Tc: crystallization temperature; Xc: degree of crystallinity.

SWCNT (wt%)	T_g (°C)	T_c (°C)	$T_{ml/II}$ (°C)	X_c (%)
0	-40.7	33.8	72.1/84.9	31.2
0.15	-36.2	54.9	77.3/85.4	41.8
0.25	-37.3	44.0	73.1/83.6	39.4
0.50	-37.0	43.9	71.3/85.1	38.2
0.65	-45.1	42.2	68.9/83.0	33.6
0.75	-42.6	42.9	72.3/85.5	35.8
0.85	-47.9	43.3	71.7/84.5	34.1
1.0	-41.5	46.1	72.6/85.5	37.7

show that the Tg (about −41°C for neat PBSA) rises slightly for low nanotube loadings (up to about 4°C) whilst decreases for high nanotube loadings. This tendency is thus unexpected, since higher nanotube contents should lead to higher crosslinking density and increased interaction with the matrix via hydrogen bonding, polar and CH-π interactions, which should be reflected in higher Tg values. This decrease in Tg has been previously reported for other polymer/SWCNT nanocomposites, ascribed to the bundling tendency of the CNTs (Marom and Wagner, 2020, Marom, 2023). Thus, the presence of CNT aggregates will lead free volumes among the polymer chains, hence is not effective in restricting chain mobility. The effect of CNT aggregates would be more significant than the hydrogen bonding, and the overall result is a drop in the transition temperature. Further, the presence of aggregates will make the nanocomposite to behave like a microcomposite, and in solutions they are expected to exhibit colligative properties, where the effective parameter in determining a physical property, such as the glass

transition temperature, is the ratio of the number of solute particles (CNTs) to the number of solvent (polymer).Thus, the glass transition will decrease with increasing CNT loading.

Conversely, at low SWCNT contents, the nanotubes are homogenously and randomly dispersed within the composite, hence are more effective in restricting chain mobility, and the Tg raises. Further, the level of crystallinity of the nanocomposites with low CNT loadings is significantly higher than that of the matrix, another factor that would contribute to the Tg increment (Marom, 2023). Similar change from increase to reduction in the Tg upon increasing nanofiller loading has been previously reported for PBSA/ attapulgite nanocomposites. Thus, it is confirmed that the state of SWCNT dispersion plays a key role on the final thermal nanocomposite properties (Qi et al., 2013).

With regard to the Tc, which is about 34ºC for neat PBSA, a clear rise is observed for all the nanocomposites, indicative that the SWCNTs act as heterogenous nucleating agents and promote the crystallization rate of the matrix, as reported previously for other polyester matrices (Díez-Pascual, 2017). Interestingly, the highest Tc increase (around 20ºC) is found for the nanocomposite with the lowest nanotube loading, whereas higher contents result in moderate increments (i.e. 9–12ºC). These results point that the nucleation effect is not proportional to the nanotube content, suggesting that a saturation level is reached particularly at higher nanotube loadings. Further, a competition between super-nucleation and confinement effects has been reported for CNT-reinforced polyester matrices (Müller et al., 2011), and one or the other can prevail depending on the nanofiller concentration. At low contents the super-nucleation effect clearly dominates, whilst at higher loadings the nanofillers can block the mobility of the polymer chains and prevent the ordered alignment of the macromolecular segments, known as confinement effect, and this would also influence the crystallization of the polymer. Further, the very well dispersed nanotubes at low loadings would lead to more nucleation sites and would be more effective in enhancing the crystallization of the matrix, whereas at higher contents the presence of aggregates would reduce the effective nucleating points, thus the overall outcome is only a moderate rise in Tc (Dubnikova et al., 2010).

Focusing on the melting temperature, the second heating DSC show that all the samples exhibit double melting behaviour due to melting, recrystallization and re-melting during heating with the higher temperature peak attributed to recrystallization process (Wang et al., 2011). Different lamellar thickness and perfection may be another explanation of the double melting peak as well as the different molecular weight species and orientations. The melting peaks of the nanocomposites were in general sharper than those of neat PBSA, indicating that the crystals of the nanocomposites are more regular. Further, Tm1 of nanocomposites with low loadings was higher than that of neat PBSA, whilst that of high loadings was similar or only slightly higher. Since Tm1 is associated with the originally grown crystals, it thus suggests the SWCNTs enhanced the stability of PBSA crystals in the nanocomposite. Conversely, Tm2, which would correspond to the melting of the crystallites formed through the melting-recrystallization of the original lamellae during the heating process (Wang et al., 2011), was hardly affected by the incorporation of the SWCNTs. Similar trend in the two melting temperatures was reported for PBSA/halloysite nanotube nanocomposites (Chiu, 2017).

4.5. Experimental mechanical properties of the nanocomposites

Table S1-S3 gather the results of the tensile and impact strength tests for nanocomposites with different SWCNT loadings prepared under different ultrasonication conditions. The ultrasonication process is crucial in the preparation of carbon nanotube-reinforced polymer nanocomposites. The ultrasonication parameters used for dispersing functionalized CNTs should be carefully evaluated to verify their effectiveness. The efficiency of debundling, is critically dependent on the sonication time and amplitude (Cheng et al., 2010). However, ultrasonication also induces defects and even scission of the tubes, which would negatively affect the CNT properties. Accordingly, it has been reported that sonication-induced cutting results in the mean tube length decaying as $t^{-1/2}$ (Hennrich et al., 2007). Thus, to optimize the preparation process PBSA/SWCNT nanocomposites, different ultrasonication times and amplitudes were tested, and their mechanical properties were evaluated (Fig. 6). Clearly, the modulus rises with increasing sonication time up to 5 min and sonication amplitude up to 85 % and then decreases slightly (Fig. 6a). Regarding the tensile strength, the trend observed in not so clear, but the highest values are obtained also for 5 min and amplitudes of 80 and 85 % (Fig. 6b). Conversely, the best results for the elongation at break and impact strength are found for shorter sonication times (i.e. 1 or 2 min) and an amplitude of 80 %, followed by an amplitude of 85 % (Fig. 6c and). Nonetheless, sonication times of 5 min at amplitudes of 80 or 85 % also lead to good results in terms of ductility and toughness. Overall, to attain an optimal balance of properties, an ultrasonication amplitude of 85 % and time of 5 min were chosen.

Generally, almost all the previous studies have demonstrated that CNTs introduced in small proportions in matrix composites could significantly enhance the nanocomposite mechanical properties (Ali et al., 2023). Such improvements can be further enhanced by functionalizing their surfaces to provide chemical compatibility with the matrix. The improved properties can be classified into improved load-carrying capability and better dispersibility of CNTs. Identical dispersion of CNT establishes mechanical interlocking within the matrix and fibre by “bridging” (Soni and Thomas, 2020). This bridging, in sequence, during tensile loading improves the load-carrying capability of the composites. The effect of the SWCNT loading was herein carefully investigated. Fig. 7 plots the data as a function of the SWCNT content for nanocomposites fabricated under the optimal sonication conditions, and the results are also included in Table S2. Similar trend was found for nanocomposites prepared at an ultrasonication amplitude of 85 % and time of 2 min (Table S3). The neat polymer has a stiffness of approximately 400 MPa, in good agreement with the results reported earlier (Seggiani, (2021), Qi et al., 2013). The modulus rises gradually with increasing SWCNT loading, showing a maximum at 0.65 wt% concentration and then decreases moderately (Fig. 7a). Thus, under the optimal conditions, a maximum stiffness increase of 114 % was observed for the nanocomposite with 0.65 wt% content. This increment is considerably stronger than those reported earlier for PBSA filled with higher amounts of other nanoparticles like layered double hydroxide (LDH) (Delorme et al., 2022), hydrolyzed collagens (Seggiani, 2021), attapulgite clay (Seggiani, (2021), Qi et al., 2013) and nanocrystalline cellulose (Hosseinipour et al., 2021). Further, it is also significantly stronger than that attained upon addition of 4 wt% HNT (Chiu, 2017) or 5 vol% graphene nanoplatelets *(Blejia et al., 2022)*, and comparable to that found upon addition of 20 wt% HNT *(*Chiu, 2017*)*. The exceptional modulus increment found herein can be attributed to the strong interactions between the PBSA matrix and the SWCNTs (i.e. H-bonding, polar and CH-π), as discussed earlier. This leads to a very strong interfacial adhesion between both phases, and results in a compact structure, thus restricting the movement of the polymeric chains, which in turn is reflected in enhanced rigidity. Further, the very homogenous dispersion of the SWCNTs at low loadings would promote a very efficient stress transfer to the filler and enhanced mechanical properties. In addition, functionalized CNT could become protonated during the processing process, resulting in CNT-CNT repulsion that induces debundling, hence better dispersibility, and thus improved properties (Natarajan, (2022)). Overall, our results are in agreement with former literature on CNT-reinforced polymers, corroborating the excellent mechanical reinforcing capabilities of SWCNTs (Ashrafi et al., 2012).

Focusing on the tensile strength, the trend observed was analogous to that described above for the modulus (Fig. 7b), with the highest increment (around 12 %) at 0.5 and 0.65 wt% content under the optimal conditions. Similarly, for nanocomposites prepared via ultrasonication

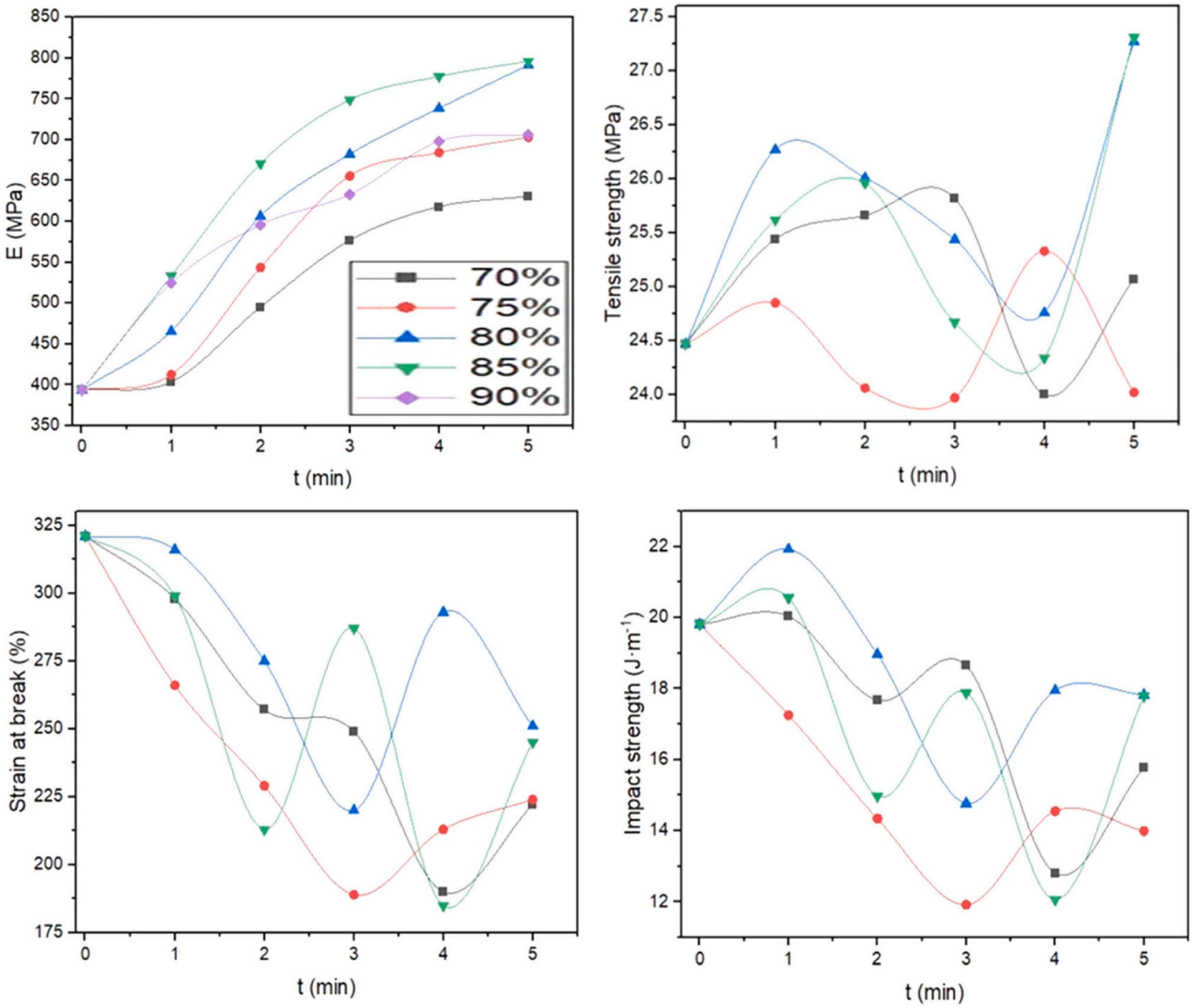

Fig. 6. Experimental mechanical properties of PBSA/SWCNT (0.5 wt%) nanocomposites as a function of ultrasonication time for different ultrasonication amplitudes.

for 2 min at 85 % amplitude, the maximum increment was about 10 % (Table S3). These increments are much smaller than those found for the modulus, although the improvements are significantly smaller. This is consistent with previous observations on SWCNT-reinforced polymers, in which the stiffness increment is typically much higher than the strength tensile strength one (Díez-Pascual et al., 2009), and could be related to the higher Young's modulus of SWCNTs compared to their strength (up to 1.25 TPa and 140 GPa, respectively (Krishnan et al., 1998). Further, the presence of defects induced during functionalization or ultrasonication stages are reported to affect more strongly to the nanotube strength (Shet et al., 2005). Nanocomposites with loadings above 0.85 % displayed lower tensile strength than the neat matrix, likely due to the nanotube agglomeration that causes stress concentrations and crack initiation. This is consistent with numerous former studies that found that adding CNT beyond ~0.5 wt% does not offer proportional enhancement in tensile properties, possibly due to CNTs aggregation (Ali et al., 2023; Soni and Thomas, 2020).

Regarding the strain at break and impact strength, the trend is opposite to the stiffness, with a gradual drop upon increasing nanotube loading, which is considerably more drastic for concentrations higher than 0.75 wt%. This is the expected trend since the nanofillers restrict the ductile flow of the polymeric chains. Further, it could also be related to the fact that chain slippage, which is characteristic for neat PBSA, is disturbed due to local shear instability caused by the introduced material heterogeneity (El-Eskandarany, 2020). Additionally, the significant decrease in load after the elastic region for the nanocomposites with high loadings could be a sign of progressive filler failure (Patti and Acierno, 2023). Based on the results obtained for the different properties, it was concluded that 0.5 wt% SWCNT content was the optimal for reinforcing PBSA matrix.

4.6. *Predicted mechanical properties using ML regression models*

Model selection is an essential phase in the development of powerful and precise predictive models in the field of ML. During the selection process, it is important to take into account the assumptions, constraints, and hyperparameters that are unique to each model. Multiple factors, such as the nature of the data, the amount of data available and the complexity of the problem have to be considered. An optimal balance between model complexity and generalization is the key to model choice. Using a suitable methodology, such as cross-validation, the candidate models are trained and evaluated after being selected. For such purpose, the available data must be divided into validation and training sets, with each model fitting on the training set before being evaluated on the validation set. Then, the models are compared using their performance metrics, and those with the highest performance are

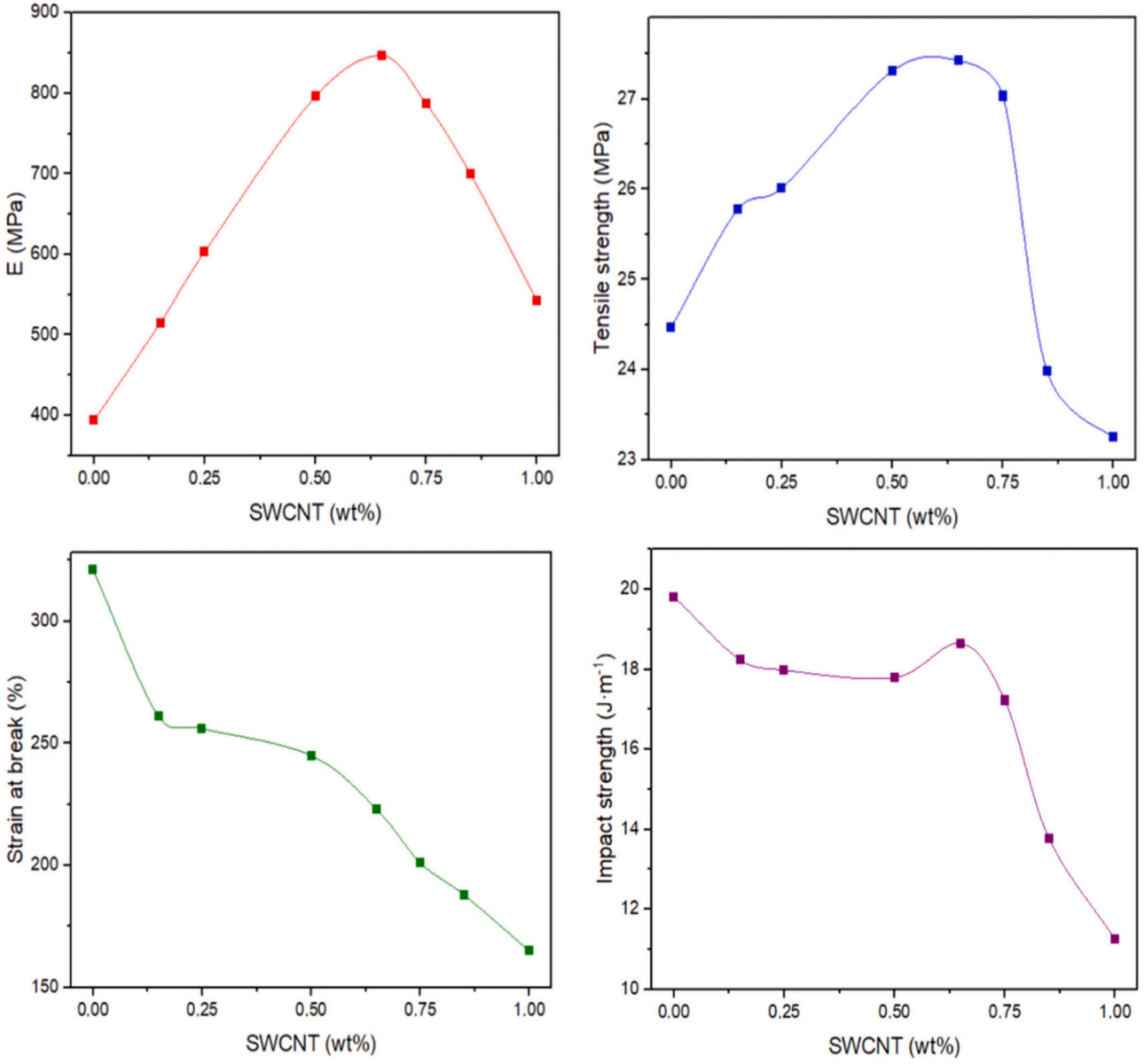

Fig. 7. Experimental mechanical properties of PBSA/SWCNT nanocomposites as a function of SWCNT loading. Samples were prepared via ultrasonication for 5 min at an amplitude of 85 %.

chosen.

Algorithms such as PR, SVR, GB and ANN have been explored and applied herein. KNN was also tested but was discarded since it did not lead to accurate results. To prepare these models for effective training, data sets containing information on the composition of the nanocomposites, expressed in terms of SWCNT percentages, were used as input data for the algorithm. In addition, values corresponding to experimental mechanical properties such as Young's modulus, tensile strength, strain at break and impact strength were considered as output data. It is important to note that the input data were not normalised and no adjustments of any kind were made to their scales.

To divide the data into training and test sets, 80 % of the data was allocated for model training, while the remaining 20 % was used for testing and evaluation. Cross-validation was applied on the training set using a k-fold cross-validation method, where k was equal to 5, to ensure robust model evaluation. To improve the performance of each algorithm in the mechanical property prediction task, specific adjustments were made to its hyperparameters. For example, in PR, the degree of the polynomial was modified. In SVR, C, gamma and epsilon parameters were adjusted. In GB, hyperparameters such as the number of estimators, the learning rate and the max Depth of the trees were tuned. In ANN, the number of neurons in the hidden layers and the learning rate were adjusted. In some cases, these adjustments were performed manually as the polynomial degree in PR, but in other situations, such as in the SVR, GB and ANN models, Randomized Search CV was used. This strategy is effective in finding the hyperparameter configuration that improves model performance without the need for testing all possible combinations, which would be costly in terms of computational resources. Randomized Search CV works by testing a random set of hyperparameter combinations and then evaluates how the model performs with each set. After a defined number of iterations, the best hyperparameter combinations were selected based on predefined performance metrics. Once the top 5 combinations were identified, trends in the hyperparameters that maximized the performance were analyzed. This information was then used to further tune the models with a Bayesian optimiser, which improved their performance.

Bayesian optimization is an effective approach that leverages probability and statistics to guide the search for the most promising

configurations, however, its performance is most outstanding when prior knowledge about the range or characteristics of hyperparameters that may be effective is gained. Thus, it is very helpful to start with Randomized Search CV and then apply Bayesian optimisation to further refine the configurations. To evaluate the hyperparameter configurations, common evaluation metrics in prediction models are used. R^2 was used to determine which of the 5 hyperparameter combinations was the most effective in each model. Once the best combination was chosen, R^2, MSE and MAE were analyzed to make an informed decision on which of the models is best suited to predict each mechanical property.

4.6.1. *Young's modulus*

-PR

To assess the impact of the polynomial degree on the performance of the model, the degree was gradually increased until the optimum value that balances the model fit and generalisability was found. As can be observed in Fig. 8, at low polynomial degrees, the model failed to capture the complexity of the data, which was reflected in relatively low R^2 values in both the training and test sets. However, as the degree of the polynomial increased, an increase in R^2 values was observed in both data sets. This indicates that the model improved its ability to fit the data and, as a result, more accurate predictions were obtained. The highest R^2 values in the training and test sets (0.9961 and 0.9888 respectively) were obtained for a degree of 4, and then remained constant, suggesting that further increasing the complexity of the model does not lead to substantial improvements in performance. Instead, it could lead to an overfitting of the model to the training data, which would negatively affect the generalisability of the model to new data. These values are better than those reported for the prediction of the Young's modulus of silicate glasses using PR model, in which for a polynomial degree of 3, R^2 for the training and test sets were 0.975 and 0.970, respectively (Yang et al., 2019). This indicates that, even in the case of a simple algorithm like polynomial regression, ML offers a good prediction of E based on the simulated results.

-SVR

The analysis of the results gathered in Table 3 shows that the hyperparameter search focuses mainly on a range of values for the hyperparameter C between 300 and 400. However, higher values of epsilon lead to a significant decrease in the R^2 values in both the training and test sets. This can be explained considering that epsilon controls the margin flexibility in the SVR model. Higher values of epsilon allow for a wider margin, which often leads to a model that fits the training and test data less accurately. Additionally, it is interesting to note that when Gamma was set to "auto", a decrease in R^2 values was observed for both sets. This may be because "auto" may lead to a too tight fit of the model, resulting in a lower generalizability. On the other hand, the use of "scale" maintains a better balance between the flexibility of the model and its ability to generalise (Zamanian et al., 2023), accounting for the higher R^2 values for both performance metrics.

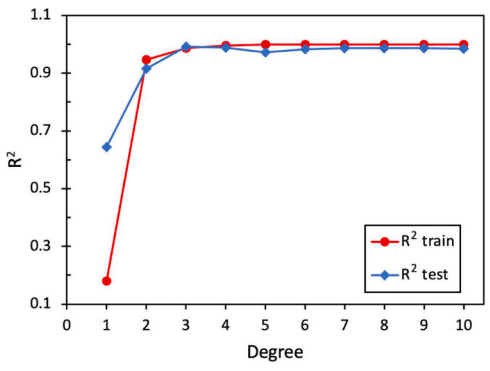

Fig. 8. R^2 in the training and test set as a function of the degree of the PR polynomial in the prediction of the Young's Modulus.

Table 3
Variation of R^2 in the training and test sets as a function of the hyperparameters in SVR, GB (decision trees) and ANN models for the prediction of the Young's Modulus.

Model	C	Epsilon	Gamma	R^2 train	R^2 test
SVR	390	0.03	scale	0.9992	0.9968
SVR	377	0.07	auto	0.5366	0.7520
SVR	360	0.01	scale	0.9985	0.9969
SVR	349	0.01	scale	0.9989	0.9969
SVR	316	0.08	auto	0.4836	0.7253
Model	Nº estimators	Max depth	Learning rate	R^2 train	R^2 test
GB	450	3	0.01	0.9998	0.6967
GB	300	5	0.3	0.7585	0.8933
GB	300	3	0.1	0.7515	0.9834
GB	200	5	0.3	0.7585	0.8934
GB	200	4	0.2	0.7585	0.8942
GB	300	5	0.3	0.7585	0.8933
Model	Nº neurons	Learning rate	R^2 train	R^2 test	
ANN	357	0.00003	0.8604	0.9869	
ANN	400	0.00003	0.9346	0.9740	
ANN	400	0.00010	0.9953	0.9047	
ANN	390	0.00010	0.9519	0.8555	
ANN	380	0.00010	0.9995	0.8750	

In a recent study (Yang et al., 2019), the mechanical properties of polyvinyl alcohol (PVA)/TiO_2/montmorillonite nanocomposites were predicted via SVR model, and R^2 values higher than 0.96 were found for the testing data. Further, studies on the prediction of the Young's modulus of self-compacting concrete using this model have also been developed (Miller et al., 2023), leading to R^2 values higher than 0.957. This corroborates that this model is accurate for predicting nanocomposite performance in terms of two independent variables, the matrix and nanofiller loadings.

In summary, high C values lead to better prediction performance, while epsilon values do not exhibit a defined trend, thus allowing for testing different options. In addition, the optimal choice for the gamma parameter to improve the model performance in terms of R^2 is to choose the "scale" setting.

-BG

Regarding BG, it is found that as the number of estimators decreases from 450 to 200, the R^2 train remains constant at around 0.7585, while R^2 test decreases slightly. R^2 train and test are maximum when the maximum tree depth is 3. This suggests that a shallower decision tree (maximum depth of 3) seems to be more suitable for this dataset, as it provides a better fit and generalisation compared to a deeper tree. Besides, as the learning rate decreases, both R^2 train and R^2 test increase. This suggests that a lower learning rate results in better performance, indicating that the model is learning more effectively at a lower learning speed. Similar conclusions were obtained for the prediction of the Young's modulus of refractory and non-refractory alloys, in which the optimal parameters were a max. depth of 3, learning rate of 0.03 and 100 estimators (Khakurel et al., 2021). Overall, a model with a moderate number of estimators, a low maximum tree depth and a low learning rate provides better performance in predicting the Young's modulus.

-ANN

According to Table 3, a higher number of neurons in the hidden layer tends to improve R^2 in the training tests, while R^2 test does not follow a trend and depends on the value of the learning rate. In general, a lower learning rate yields a higher R^2 in the test set. For example, for a learning rate of 0.00003, both R^2 train and R^2 test improve as the number of neurons in the hidden layer increase. However, this trend is reversed for a higher learning rate (0.00010). The highest R^2 test (0.9740) is obtained for 400 neurons in the hidden layer and a learning rate of 0.00003. These values provide a good balance between performance on the training set and the test set, indicating that the model generalizes well without fitting the training set. These results are better than those reported for low density polyethylene/graphene nanoplatelets composites, in which the best R^2 value for the Young's modulus was 0.933 for

13 neurons in the hidden layer (Khanam et al., 2016), and those found for ternary PEEK/Ti/C nanocomposites, with an R^2 value in the training set of 0.960 for 27 neurons in the hidden layer (Zakaulla et al., 2022).

-Choice of model

In order to determine which model is the most suitable to predict the Young's modulus, it is crucial to analyse the key metrics, namely R^2, MSE and MAE. The best combination for each model is gathered in Table S4. SVR model stands out as the most favourable choice for predicting the Young's modulus, with the highest R^2 values, and low MSE and MAE. These metrics indicate outstanding accuracy and robust generalisability of the SVR model compared to the other models. PR and ANN also exhibit high performances; conversely, BG (an ensemble algorithm based on generally shallow decision trees *(*Zhang et al., 2019*))*, is not as effective in capturing highly non-linear relationships.

It is possible to further improve the results of SVR model by applying the Bayesian optimiser, as shown in Table S5. The hyperparameters set in the optimiser are based on information previously obtained through RandomSearchCV. C was set at values higher than 390, epsilon between 0.001 and 0.1, since no clear relationship was found between its value and the model performance, and gamma was fixed at "scale" option, as this setting provided better results. The optimal combination of hyperparameters by the Bayesian optimiser are C=4000, epsilon=3 and gamma set to "scale". It is important to note that, although no improvement is observed in the training set, the performance in the test set shows a substantial enhancement, with R^2 value of 0.9999. Further, an MSE of 0.5613 and a MAE of 0.0102 were attained.

4.6.2. Tensile strength

-PR

The relationship between the degree of the polynomial and the performance of the algorithm is shown in Fig. 9. Clearly, as the degree increases, R^2 of the train test increases significantly, indicating a better fit to the training data. However, R^2 of the test set shows a different behavior: it is minimum when the degree is 1 and 4, while it increases for higher values. In general, the polynomial regression model performs poorly especially on the test set, possibly because the relationship in the data is highly non-linear and cannot be adequately approximated by a polynomial; thus, PR could provide inaccurate results and hence negative R^2 test values. It is therefore necessary to explore other modelling approaches or make improvements to the data or preprocessing

-SVR

Using SVR, it was found that R^2 in the train set tends to decrease as the value of C increases, while R^2 test tends to increase, but the values obtained are not suitable (Table 9). No clear relationship is found between epsilon and R^2 values, suggesting that this parameter does not have a significant effect on the performance of this model (Table 9),. Regarding gamma kernel coefficient, a good fit to the training data is observed when "scale" is chosen, reflected in a high R^2 train, although

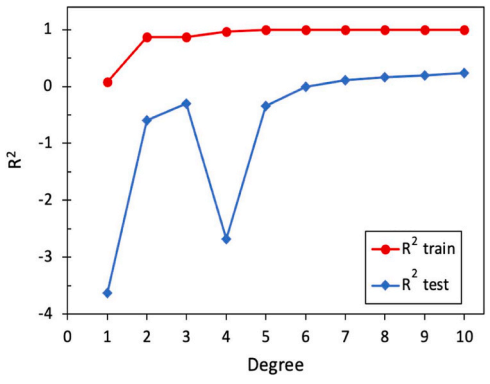

Fig. 9. R^2 in the training and test as a function of the degree of the PR polynomial in the prediction of the tensile strength.

Table 9
Variation of R^2 in training and test as a function of hyperparameters in SVR, GB and ANN models for Tensile Strength prediction.

Model	C	Epsilon	Gamma	R^2 train	R^2 test
SVR	18	0.1	scale	0.9927	-1.2082
SVR	181	0.7	auto	0.8804	-0.8183
SVR	189	0.04	auto	0.8797	0.2117
SVR	249	0.04	auto	0.8689	0.2965
SVR	479	0.04	auto	0.8755	0.2237
Model	**Max Depth**	**Learning rate**		**R^2 train**	**R^2 test**
GB	3	0.3		0.9999	0.7198
GB	7	0.2		0.9999	0.7358
GB	3	0.01		0.9999	0.7606
GB	6	0.01		0.9999	0.757
GB	4	0.2		0.9999	0.7358
Model	**Nº neurons**	**Learning rate**		**R^2 train**	**R^2 test**
ANN	100	0.0075		0.9163	0.4424
ANN	80	0.0107		0.9582	0.2679
ANN	80	0.0058		0.223	0.4216
ANN	70	0.0066		0.8621	0.5509

this is not translated into good performance in the R^2 test. In contrast, when "auto" is used, R^2 test improves considerably, indicating a better ability of the model to generalise to unseen data. SVR was used to predict the tensile strength of concrete (Ray et al., 2021), resulting in R^2 values in the training set in the range of 0.88–0.92 for C= 10,000 and epsilon 0.02. It is important to note that herein, R^2 values in the test set are low and negative in some cases, indicating poor model performance. It is therefore worthwhile to explore other alternative regression models rather than relying on the SVR model in this context.

-GB

In this model, no relationship between the number of estimators and R^2 of the train or test set is found (Table 9), although RandomSearchCv shows that the best combinations correspond to a high number of estimators. The performance also depends on other hyperparameters: as the max Depth increases, R^2 of both the train and test sets increase, with deeper decision trees performing better on both datasets. On the other hand, as the Learning Rate decreases from 0.3 to 0.01, R^2 test tends to increase. Thus, a configuration with a high number of estimators, a maximum depth of 3 and a learning rate of 0.01 provides the best performance for predicting the tensile strength in this model. Similar results were obtained for the prediction of the strength of cemented sand and gravel (Luo et al., 2023), where a max. depth of 3 and 300 estimators led to the optimum performance ($R^2 = 0.9747$)

-ANN

The performance in this model is mainly influenced by the learning rate. Low values of this parameter (0.0066, 0.0063) lead to better performance on the test set, especially 0.0063, which provides the highest R^2 and, therefore, a better generalisation ability to unseen data. On the other hand, no clear relationship between the number of neurons in the hidden layer and performance on the test set is observed. Although the optimum performance for both the training and test sets is achieved with a learning rate of 0.0063 and 70 neurons in the hidden layer, these results are still not good enough. Therefore, other parameters could be tested to further improve the performance of the model.

Table S6 lists the hyperparameter combinations that provide a good balance between performance in the training set and the test set for each model. Based on these results and the evaluation of various metrics, such as R^2, MSE of 0.0003, and MAE of 0.3008, it can be concluded that the GB algorithm is the preferred choice for the prediction of tensile strength. Furthermore, this algorithm has demonstrated its consistency in accurately this property in previous studies (Jayasudha et al., 2022, de-Prado-Gil et al., (2022)). Therefore, GB is presented as a robust and reliable choice, since this method helps to prevent the problem of over-fitting to some extent, and solves the problems of a non-linear relation between target properties and features as well as to deal with

the collinearity among the features. In a recent study, it was found that among 8 ML models, GB had the best predictive strength (Zhang et al., 2019).

In addition, Table S7 compares the experimental and predicted values for both the training and test sets. It is important to highlight that, upon application of the Bayesian optimiser, taking advantage of the information collected during the initial search with randomSearchCV, significant improvements in the accuracy of the predictions were attained in both data tests. The number of estimators was set above 400, while the learning rate ranged from 0.001 to 0.1, and the max depth from 1 to 5. Finally, the Bayesian optimizer has identified the optimal hyperparameters as follows: a number of estimators of 639, a maximum depth of 2, and a learning rate of 0.045. This optimisation has contributed positively to the quality of the predictions in both datasets, with R^2 of 1 on the training set and 0.7358 on the test set, an MSE of $2.1268e^{-16}$, and a MAE of 0.3150.

4.6.3. Elongation at break

-PR

The results of the PR analysis plotted in Fig. 10 reveal remarkable trends. As the degree of the polynomial increases, the performance on the training set increases gradually and reaches a maximum value of 1 from a degree of 5 onwards, indicating a perfect fit to the training data. However, R^2 on the test set also rises up to a degree of 5, and then decreases slightly. This decline suggests that the PR model begins to overfit the data, which may lead to somewhat poor performance on new or unseen data. Therefore, it is important to select the degree of the polynomial carefully to set a balance between an accurate fit and the generalisability of the model. The best results for both the training set and the test set are obtained for a degree of 5, leading to R^2 values of 1 and 0.9888, respectively.

-SVR

The results in Table 10 show that, in general, as the C value increases, R^2 in the train set tends to increase, while R^2 test varies without following a trend. Epsilon parameter does not have a clear influence on the performance of the model, as different epsilon values (0.7, 0.3, 0.01) do not show a definite trend in terms of R^2 train or R^2 test. The "scale" configuration for gamma seems to stand out again, leading to the best performances. The best results are observed when C is set to 119, epsilon to 0.3 and gamma to scale. These values provide the right balance between fit to the training data and generalisability to unseen data, resulting in a high R^2 test

-GB

No clear trend in R^2 as a function of the number of estimators is found. However, RandomSearchCV performs better in a range of values between 100 and 500 (Table 10). A maximum depth of 6 or higher leads to the highest R^2 in the test set. Low learning rates of 0.001 and 0.01 produce good test set performances. The optimal balance between R^2 train and test (0.8239 and 0.5041, respectively) is found for 200 estimators, a maximum depth of 4 and a learning rate of 0.01. Despite this, it is important to consider exploring other algorithms to further improve the results.

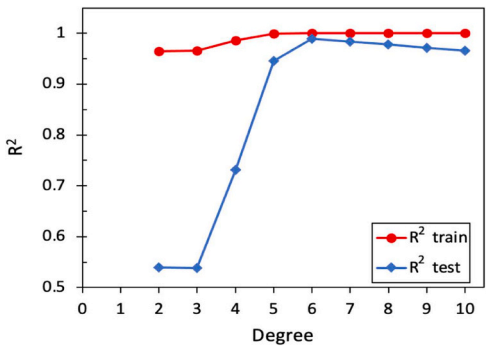

Fig. 10. R^2 in training and test sets as a function of the degree of the PR polynomial in the prediction of the elongation at break.

Table 10
Variation of R^2 in training and test as a function of hyperparameters in SVR, GB and ANN for elongation at break prediction.

Model	C	Epsilon	Gamma	R^2 train	R^2 test
SVR	439	0.7	auto	0.7136	0.8326
SVR	162	0.7	scale	0.9987	0.7750
SVR	119	0.3	scale	0.9921	0.8163
SVR	67	0.01	scale	0.8854	0.9768
SVR	10	0.7	scale	0.7136	0.8326
Model	Nº estimators	Max Depth	Learning rate	R^2 train	R^2 test
GB	500	3	0.01	0.8432	0.3241
GB	500	4	0.001	0.5826	0.5209
GB	200	5	0.2	0.8433	0.3110
GB	200	4	0.01	0.8239	0.5041
GB	100	6	0.01	0.7873	0.7474
Model	Nº neurons	Learning rate	R^2 train	R^2 test	
ANN	400	0.00032	0.9367	0.8926	
ANN	350	0.00023	0.9235	0.9503	
ANN	350	0.00001	0.9278	0.9211	
ANN	300	0.00006	0.9349	0.8943	
ANN	172	0.00031	0.9349	0.8941	

-ANN

In general, the performances obtained with this model are good (R^2 >0.89 and 0.92 in the test and train sets, respectively). No tendency is identified with the number of neurons in the hidden layer, ranging between 400 and 172. On the other hand, learning rates of 0.00001 and 0.00023 produce higher R^2 test.

Specifically, according to the Table, the best combination of values is attained for a learning rate of 0.00001 and 350 neurons in the hidden layer, which results in R^2 train of 0.9278 and R^2 test of 0.9211. These results are better than those reported for the prediction of the elongation at break of ternary PEEK/Ti/C nanocomposites using an ANN model with 27 neurons in the hidden layer, that led to an R^2 value of the training set equal to 0.94 (Zakaulla et al., 2022).

The optimal combinations for each algorithm are summarized in Table S8, and their performances are evaluated using metrics such as R^2, MSE and MAE. Accordingly, it can be concluded that PR is the preferred algorithm due to its higher R^2 and lower MSE and MAE values. Furthermore, PR is a suitable choice due to its simplicity, intuitively, and low computational cost (Qu et al., 2021). Further, the experimental values are compared with the predictions generated by this algorithm in Table S9. In this case, no significant improvement was achieved by applying the Bayesian optimiser.

4.6.4. Impact strength

-PR

R^2 train values obtained by the PR algorithm are high for the degrees of the polynomial tested, suggesting a robust fit to the training data (Fig. 11). However, the corresponding R^2 test values are negative, indicating a very poor performance in the generalisability of the model to unseen data. This discrepancy between R^2 train and test sets points to a problem of overfitting the model to the training data and, as a result, it has difficulties in making accurate predictions on unseen data within the range of 1–10.

-SVR

The results obtained with this model are collected in Table 11. High R^2 train values are obtained, indicating a good fit to the training data. However, the corresponding R^2 test values are negative, reflecting very poor performance when applying the model to unseen data. Thus, other algorithms should be tested to attain better generalisability and prediction performance.

-BG

The trend is similar to that mentioned above for the SVR algorithm

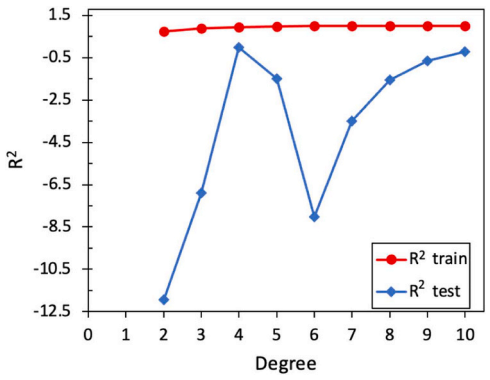

Fig. 11. R^2 in the training and test sets as a function of the degree of the PR polynomial in the prediction of the impact strength.

Table 11
Variation of R^2 in training and test as a function of hyperparameters in SVR, GB and ANN for impact strength prediction.

Model	C	Epsilon	Gamma	R^2 train	R^2 test
SVR	329	0.8	auto	0.9053	-3.0879
SVR	315	0.9	auto	0.9	-2.7393
SVR	233	0.01	scale	1	-1.5046
SVR	159	0.07	auto	0.9013	-4.6635
SVR	17	0.01	scale	0.9886	-1.8463

Model	Nº estimators	Max Depth	Learning rate	R^2 train	R^2 test
GB	500	5	0.01	1	-2.9948
GB	500	4	0.3	1	-4.7705
GB	450	3	0.01	0.9999	-2.9553
GB	400	6	0.3	1	-3.0609
GB	200	4	0.2	1	-3.0609

Model	Nº neurons	R^2 train	R^2 test
ANN	80	0.9557	0.9223
ANN	70	0.9665	0.7413
ANN	50	0.9669	0.7764
ANN	50	0.9659	0.7383
ANN	50	0.959	0.9051

(Table 11). The results on the training set are consistently high, with values close to 1, but the performance on the test set is consistently negative, indicating poor performance in generalising to unseen data, regardless of the various combinations of hyperparameters used.

-ANN

Interestingly, as the number of neurons in the hidden layer decreases, R^2 train tends to increase, while R^2 test decreases very sharply, for example, from 80 to 70 neurons in the hidden layer. However, low learning rates lead to better R^2 test compared to high ones. A low learning rate allows the model to converge more stably and avoids excessive oscillations during training, leading to better generalization. In summary, an outstanding balance between the training and the test set (R^2 values of 0.9557 and 0.9223, respectively) can be achieved using a high number of neurons in the hidden layer (Bozeya et al., 2021) together with a low learning rate (0.0080). This is reflected in a robust test set, indicating outstanding performance in model fitting and generalisation.

The best hyperparameter configurations for each model are collected in Table S10. It can be concluded that the only model that stands out is ANN, with high values of R^2, as well as low values of MSE and MAE, offering excellent predictive ability with minimal errors. In this case, the use of the Bayesian optimiser did not have a significant impact on the improvement of the results. However, the comparison between the real values and the predictions in the training and test sets shows remarkable closeness (Table S11), although the results are not as exceptional as those obtained for the prediction of the mechanical properties mentioned above. ANNs have a higher modelling capability and can learn more complex representations of the data (Khan et al., 2009), allowing them to tackle more challenging problems such as impact strength prediction.

5. Conclusions

In this study, bionanocomposites based on PBSA copolyester reinforced with different loadings of polyaminobenzenesulfonic acid functionalized SWCNTs (0.15–1 wt%) have been prepared through a straightforward solution casting method. Different ultrasonication times and amplitudes have been tested in order to determine the optimal conditions (5 min and 85 % amplitude). SEM analysis corroborated the uniform and random distribution of the SWCNTs at low loadings, while aggregates were observed at concentrations higher than 0.65 wt%. FTIR suggested strong interactions between the ester groups of the polymer and the amino groups and the sulphonic acid moieties of the SWCNTs via hydrogen bonding and polar interactions, as well as CH-π interaction between the hydrocarbon chain of the polyester and the aromatic rings of the SWCNTs. The nanofillers had a heterogenous nucleating effect, increasing the crystallization temperature of the polymer at low nanotube loadings (by around 20ºC), whilst the melting temperature of the polymer was hardly modified. They also increased the glass transition temperature of the matrix (by about 4ºC), at low loadings, whereas it was reduced at higher concentrations due to nanotube agglomeration. The thermal stability of the matrix remained merely unchanged upon incorporation of the SWCNTs. Further, unprecedent increments in stiffness were found upon incorporation of the SWCNTs, up to 114 % for the nanocomposite with 0.65 wt% content. This increment is considerably stronger than those reported earlier for PBSA filled with higher amounts of other nanoparticles, attributed to a very effective load transfer between the two composite phases. Conversely, the ductility and impact strength were reduced at high SWCNT concentrations. Thus, the composite with 0.5 wt% SWCNTs shows the optimal balance of properties, showing about 2-fold increment in stiffness, 11 % improvement in strength and just a slight reduction (about 7 %) in impact strength. The mechanical properties have been accurately predicted using PR, SVR, GB and ANN models. Regarding the Young's modulus estimation, SVR demonstrated exceptional performance, with a R^2 of 0.9992 and 0.9968 in the training and test set, respectively. For the tensile strength, GB excelled with a R^2 of 0.9999 and 0.7606 in the indicated sets, a MSE of 0.0003, and a MAE of 0.3008. In the case of elongation at break, PR showed outstanding performance with R^2 of 1 in the training set and 0.9998 in the test set. ANN was highly effective in predicting impact resistance, with a R^2 of 0.9557 and 0.9223 in the training and test sets, respectively, MSE of 0.3425 and MAE of 0.5818. Additionally, thanks to the information obtained by CV random search, the Bayesian optimizer was able to further optimize the prediction of the Young's modulus and tensile strength with the selected algorithms. Overall, the results confirm that the developed models are highly suitable for predicting the mechanical properties of carbon nanotube-reinforced polymeric nanocomposites, which is valuable to expand their applications in fields such as biomedicine, pharmaceutical industries and food packaging. Overall, ML models can provide higher efficiency, accuracy, and cost savings in the design and optimization of polymer nanocomposites, making them a highly interesting and vibrating field of study.

Funding

Financial support from Alcalá University is gratefully acknowledged (PIUAH23/CC-046). M.E.G.M and V.S. would like to thank the Ministerio de Ciencia e Innovación (Spain) and the European Community (PID2021-122708OB-C31 and grant number: RYC2021-033921-I) for the financial support.

CRediT authorship contribution statement

Pilar Garcia-Diaz: Writing – original draft, Supervision. **Elizabeth Champa-Bujaico:** Formal analysis, Data curation. **Marta E. Mosquera:** Writing – review & editing. **Valentina Sessini:** Writing – original draft, Data curation. **Ana M. Díez-Pascual:** Conceptualization, Methodology, Writing – review & editing.

Declaration of Competing Interest

The authors declare that they have no known competing financial interests or personal relationships that could have appeared to influence the work reported in this paper.

Data Availability

Data will be made available on request.

Appendix A. Supporting information

Supplementary data associated with this article can be found in the online version at doi:10.1016/j.indcrop.2024.119018.

References

Abraham, A., 2005. Artificial neural networks. Handb. Meas. Syst. Des. https://doi.org/10.1002/0471497398.mm421.

Aler, R., Galván, I.M., Ruiz-Arias, J.A., Gueymard, C.A., 2017. Improving the separation of direct and diffuse solar radiation components using machine learning by gradient boosting. Sol. Energy 150, 558–569. https://doi.org/10.1016/j.solener.2017.05.018.

Ali, A., Koor, S.S.R., Alshehri, A.H., Arockiarajan, A., 2023. Carbon nanotube characteristics and enhancement effects on the mechanical features of polymer-based materials and structures – A review. J. Mater. Res. Technol. 24, 6495–6521.

Anifowose, F.A., Eludiora, S., 2002. Application of Artificial Intelligence in Network Intrusion Detection: A Succinct Review. Comput. Sci. 158.

Antolin-Ceron, V.H., Gonzalez-Jauregui, D., Astudillo-Sanchez, P.D., Cabrera-Chavarria, J., Andrade-Melecio, H.A., Barrera-Rivera, K.A., Martinez-Richa, A., 2023. Influence of carbon nanotube functionalization on the physical properties of PCL diol/chitosan blends. J. Chem. Technol. Biotechnol. (1986) 98, 1673–1689. https://doi.org/10.1002/jctb.7389.

Ashrafi, B., Díez-Pascual, A.M., Johnson, L., Genest, M., Hind, S., Martinez-Rubi, Y., González-Domínguez, J.M., Teresa Martínez, M., Simard, B., Gómez-Fatou, M.A., Johnston, A., 2012. Processing and properties of PEEK/glass fiber laminates: Effect of addition of single-walled carbon nanotubes. Compos., Part A 43, 1267–1279. https://doi.org/10.1016/j.compositesa.2012.02.022.

Babu, R.P., O'Connor, K., Seeram, R., 2013. Current progress on bio-based polymers and their future trends. Prog. Biomater. 2, 8–16. https://doi.org/10.1186/2194-0517-2-8.

Bafandeh Imandoust, S., Bolandraftar, M., 2013. Application of K-nearest neighbor (KNN) approach for predicting economic events theoretical background. J. Eng. Res. Appl. 3, 605–610.

Berner, J., Elbrächter, D., Grohs, P., 2019. How degenerate is the parametrization of neural networks with the ReLU activation function?

Biau, G., Devroye, L., 2010. On the layered nearest neighbour estimate, the bagged nearest neighbour estimate and the random forest method in regression and classification. J. Multivar. Anal. 101, 2499–2518. https://doi.org/10.1016/j.jmva.2010.06.019.

Bleija, M., Platnieks, O., Macutkevič, J., Starkova, O., Gaidukovs, S., 2022. Comparison of Carbon-Nanoparticle-Filled Poly(Butylene Succinate-co-Adipate) Nanocomposites for Electromagnetic Applications. Nanomaterials 12, 3671. https://doi.org/10.3390/nano12203671.

Bock, F.E., Aydin, R.C., Cyron, C.J., Huber, N., Kalidindi, S.R., Klusemann, B., 2019. A Review of the Application of Machine Learning and Data Mining Approaches in Continuum Materials Mechanics. Front. Mater. 6. https://doi.org/10.3389/fmats.2019.00110.

Bozeya, A., Makableh, Y.F., Abu-Zurayk, R., Khalaf, A., Al Bawab, A., 2021. Thermal and structural properties of high density polyethylene/carbon nanotube nanocomposites: a comparison study. Chemosensors 9, 136. https://doi.org/10.3390/chemosensors9060136.

Brunner, C.T., Baran, E.T., Pinho, E.D., Reis, R.L., Neves, N.M., 2011. Performance of biodegradable microcapsules of poly(butylene succinate), poly(butylene succinate-co-adipate) and poly(butylene terephthalate-co-adipate) as drug encapsulation systems. Colloids Surf., B: Biointerfaces 84, 498–507. https://doi.org/10.1016/j.colsurfb.2011.02.005.

Buxbaum, L.H., 1968. The Degradation of Poly(ethylene terephthalate), 7, 182–190 Angew. Chem. Int. Ed. Engl. 7, 182–190. https://doi.org/10.1002/anie.196801821.

Canas, J.E., Long, M., Nations, S., Vadan, R., Dai, L., Luo, M., Ambikapathi, R., Lee, E.H., Olszyk, D., 2008. Effects of functionalized and nonfunctionalized single-walled carbon nanotubes on root elongation of select crop species. Environ. Toxicol. Chem. 27, 1922–1931. https://doi.org/10.1897/08-117.1.

Cencer, M.M., Moore, J.S., Assary, R.S., 2022. Machine learning for polymeric materials: an introduction. Polym. Int. 71, 537–542. https://doi.org/10.1002/pi.6345.

Champa-Bujaico, E., García-Díaz, P., Díez-Pascual, A.M., 2022. Machine Learning for Property Prediction and Optimization of Polymeric Nanocomposites: A State-of-the-Art. Int. J. Mol. Sci. 23, 10712. https://doi.org/10.3390/ijms231810712.

Chen, J.-Y., Zhang, X.-W., Wu, T.-Y., Ye, H.-M., 2023. Co-Crystallization between Aliphatic Polyesters through Co-Inclusion Complexation with Small Molecule. Mol. (Basel, Switz.) 28, 4091. https://doi.org/10.3390/molecules28104091.

Cheng, Q., Debnath, S., Gregan, E., Byrne, H.J., 2010. Ultrasound-Assisted SWNTs Dispersion: Effects of Sonication Parameters and Solvent Properties. J. Phys. Chem. C. 114, 8821–8827. https://doi.org/10.1021/jp101431h.

Chiu, F.-C., 2017. Halloysite nanotube- and organoclay-filled biodegradable poly (butylene succinate-co-adipate)/maleated polyethylene blend-based nanocomposites with enhanced rigidity. Compos., Part B 110, 193–203. https://doi.org/10.1016/j.compositesb.2016.10.09.

Ciecierska, E., Boczkowska, A., Kurzydlowski, K.J., Rosca, I.D., Van Hoa, S., 2013. The effect of carbon nanotubes on epoxy matrix nanocomposites. J. Therm. Anal. Calorim. 111, 1019–1024. https://doi.org/10.1007/s10973-012-2506-0.

Cristianini, N., Shawe-Taylor, J., 2002. An introduction to support vector machines and other kernel-based learning methods. Cambridge Univ. Press, Cambridge [u.a.]. ⟨https://doi.org/10.1017/CBO9780511801389⟩.

Delorme, A.E., Radusin, T., Myllytie, P., Verney, V., Askanian, H., 2022. Enhancement of Gas Barrier Properties and Durability of Poly(butylene succinate-co-butylene adipate)-Based Nanocomposites for Food Packaging Applications. Nanomaterials 12, 978. https://doi.org/10.3390/nano12060978.

de-Prado-Gil, J., Palencia, C., Jagadesh, P., Martínez-García, R., 2022. A Comparison of Machine Learning Tools That Model the Splitting Tensile Strength of Self-Compacting Recycled Aggregate Concrete. Materials 15, 4164. https://doi.org/10.3390/ma15124164.

Diez-Pascual, A.M., 2017. Tissue Engineering Bionanocomposites Based on Poly (propylene fumarate). Polymers 9, 260. https://doi.org/10.3390/polym9070260.

Díez-Pascual, A.M., 2021. Chemical Functionalization of Carbon Nanotubes with Polymers: A Brief Overview. Macromol 1, 64–83. https://doi.org/10.3390/macromol1020006.

Díez-Pascual, A.M., Naffakh, M., Gómez, M.A., Marco, C., Ellis, G., González-Domínguez, J.M., Ansón, A., Martínez, M.T., Martínez-Rubi, Y., Simard, B., Ashrafi, B., 2009. The influence of a compatibilizer on the thermal and dynamic mechanical properties of PEEK/carbon nanotube composites. Nanotechnology 20, 315707. https://doi.org/10.1088/0957-4484/20/31/315707.

Drew, P.J., Monson, J.R.T., 2000. Artificial neural networks. Surgery 127, 3–11. https://doi.org/10.1067/msy.2000.102173.

Dubnikova, I., Kuvardina, E., Krasheninnikov, V., Lomakin, S., Tchmutin, I., Kuznetsov, S., 2010. The effect of multiwalled carbon nanotube dimensions on the morphology, mechanical, and electrical properties of melt mixed polypropylene-based composites. J. Apply. Polym. Sci. 117, 259–272. https://doi.org/10.1002/app.31979.

El-Eskandarany, M.S., 2020. Ball milling as a superior nanotechnological fabrication's tool, Mechanical Alloying. Elsevier Science & Technology Books, United States.

Freund, Y., Schapire, R. E., 1999. A Short Introduction to Boosting (Special Issue: "Recent Dvelopments in the Theory and Applications of Machine Learning"). J. Jpn. Soc. Artif. Intell. 14, 771–780. https://doi.org/10.11517/jjsai.14.5_771.

Friedman, J.I., Hastie, T., Tibshirani, R., 2001. The elements of statistical learning: data mining, inference, and prediction, 1st ed, Springer Series in Statistics. Springer, New York, NY. ⟨https://doi.org/10.1007/978-0-387-21606-5⟩.

Fukushima, K., Wu, M.-H., Bocchini, S., Rasyida, A., Yang, M.-C., 2012. PBAT based nanocomposites for medical and industrial applications. Mater. Sci. Eng. C. 32, 1331–1351. https://doi.org/10.1016/j.msec.2012.04.005.

Gavin, H.P., 2023. The Levenberg-Marquardt algorithm for nonlinear least squares curve-fitting problems. Mathematics, Comput. Sci.

González-Gaitán, C., Ruiz-Rosas, R., Morallón, E., Cazorla-Amorós, D., 2015. Functionalization of carbon nanotubes using aminobenzene acids and electrochemical methods. Electroactivity for the oxygen reduction reaction. Int. J. Hydrog. Energy 40, 11242–11253. https://doi.org/10.1016/j.ijhydene.2015.02.070.

Guégan, D., Huck, N., 2005. On the use of Nearest Neighbors in finance. Financ. (Paris) 26, 67–86. https://doi.org/10.3917/fina.262.0067.

Guenther, N., Schonlau, M., 2016. Support Vector Machines. Stata J. 16, 917–937. https://doi.org/10.1177/1536867X1601600407.

Hagan, M.T., Menhaj, M.B., 1994. Training feedforward networks with the Marquardt algorithm. IEEE Trans. Neural Netw. 5, 989–993. https://doi.org/10.1109/72.329697.

Hayashi, M., Tournilhac, F., 2017. Thermal stability enhancement of hydrogen bonded semicrystalline thermoplastics achieved by combination of aramide chemistry and supramolecular chemistry. Polym. Chem. 8, 461–471. https://doi.org/10.1039/C6PY01833E.

Heiberger, R.M., Neuwirth, E., 2009. In: Use, R. (Ed.), R Through Excel: A Spreadsheet Interface for Statistics, Data Analysis, and Graphics, 1st ed. Springer New York, New York, NY. https://doi.org/10.1007/978-1-4419-0052-4.

Hennrich, F., Krupke, R., Arnold, K., Rojas Stütz, J.A., Lebedkin, S., Koch, T., Schimmel, T., Kappes, M.M., 2007. The Mechanism of Cavitation-Induced Scission of Single-Walled Carbon Nanotubes. J. Phys. Chem. B. 111, 1932–1937. https://doi.org/10.1021/jp065262n.

Hexig, A., Hexig, B., 2012. Characterization of Compositional Gradient Structure of Polymeric Materials by FTIR Technology. Mater. Sci. Technol. https://doi.org/10.5772/34674.

Hosseinipour, A., Abdolrasouli, M., Mirzai, M., 2021. Bioplastic Nanocomposites Based on Polybutylene Succinate Adipate (PBSA)/Aminosilane Modified Nonocrystalline. Cellul.: Struct., Therm. Phys. Prop. Iran. J. Polym. Sci. Technol. 34, 499. https://doi.org/10.22063/JIPST.2022.3020.2104.

Hsu, C.-W., Lin, C.-J., 2002. A comparison of methods for multiclass support vector machines. IEEE Trans. Neural Netw. 13, 415–425. https://doi.org/10.1109/72.991427.

Huang, J.C., Ko, K.M., Shu, M.H., Hsu, B.M., 2020. Application and comparison of several machine learning algorithms and their integration models in regression problems. Neural Comput. Appl. 32 (10), 5461–5469. https://doi.org/10.1007/s00521-019-04644-5.

Imran, M.S., Go, G.-M., Hussain, M., Al-Harthi, M.A., 2022. Multiwalled Carbon Nanotube-Coated Poly-Methyl Methacrylate Dispersed Thermoplastic Polyurethane Composites for Pressure-Sensitive Applications. Macromol 2, 211–224. https://doi.org/10.3390/macromol2020014.

Jayasudha, M., Elangovan, M., Mahdal, M., Priyadarshini, J., 2022. Accurate Estimation of Tensile Strength of 3D Printed Parts Using Machine Learning Algorithms. Processes 10, 1158. https://doi.org/10.3390/pr10061158.

Ji, Y., Yang, X., Ji, Z., Zhu, L., Ma, N., Chen, D., Jia, X., Tang, J., Cao, Y., 2020. DFT-Calculated IR Spectrum Amide I, II, and III Band Contributions of N-Methylacetamide Fine Components. ACS Omega 5, 8572–8578. https://doi.org/10.1021/acsomega.9b04421.

Joseph, J., Jemmis, E.D., 2007. Red-, Blue-, or No-Shift in Hydrogen Bonds: A Unified Explanation. J. Am. Chem. Soc. 129, 4620–4632. https://doi.org/10.1021/ja067545z.

Khakurel, H., Taufique, M.F.N., Roy, A., Balasubramanian, G., Ouyang, G., Cui, J., Johnson, D.D., Devanathan, R., 2021. Machine Learning Assisted Prediction of the Young's Modulus of Compositionally Complex Alloys. Sci. Rep. 11, 17149. https://doi.org/10.1038/s41598-021-96507-0.

Khan, A., Shamsi, M.H., Choi, T.-S., 2009. Correlating dynamical mechanical properties with temperature and clay composition of polymer-clay nanocomposites. Comput. Mater. Sci. 45, 257–265. https://doi.org/10.1016/j.commatsci.2008.09.027.

Khanam, P.N., AlMaadeed, M., AlMaadeed, S., Kunhoth, S., Ouederni, M., Sun, D., Hamilton, A., Jones, E.H., Mayoral, B., 2016. Optimization and Prediction of Mechanical and Thermal Properties of Graphene/LLDPE Nanocomposites by Using Artificial Neural Networks. Int. J. Polym. Sci. 2016, 1–15. https://doi.org/10.1155/2016/5340252.

Koronis, G., Silva, A., Fontul, M., 2013. Green composites: A review of adequate materials for automotive applications. Compos., Part B, Eng. 44, 120–127. https://doi.org/10.1016/j.compositesb.2012.07.004.

Kramer, O., 2013. Dimensionality reduction with unsupervised nearest neighbors, 1st ed, Intelligent systems reference library. Springer, Berlin; Heidelberg [u.a.]. ⟨https://doi.org/10.1007/978-3-642-38652-7⟩.

Krishnan, A., Dujardin, E., Ebbesen, T.W., Yianilos, P.N., Treacy, M.M.J., 1998. Young's modulus of single-walled nanotubes. Phys. Rev. B Condens 58, 14013–14019. https://doi.org/10.1103/PhysRevB.58.14013.

Le, T.-T., 2021. Prediction of tensile strength of polymer carbon nanotube composites using practical machine learning method. J. Compos. Mater. 55, 787–811. https://doi.org/10.1177/0021998320953540.

Levy Mangin, J.-P., Florez Lopez, R., Fernandez Fernandez, J.M., 2008. Las redes neuronales artificiales. Fundamentos teóricos y aplicaciones prácticas. Netbiblo. https://doi.org/10.4272/978-84-9745-246-5.

Li, H., Liang, Y., Xu, Q., 2009. Support vector machines and its applications in chemistry. Chemom. Intel. Lab. Syst. 95, 188–198. https://doi.org/10.1016/j.chemolab.2008.10.007.

Li, Z., Wilkins, S.J., Moon, K.S., Wong, C.P., 2012. Carbon Nanotubes/Polymer Nanocomposites: Improved or Reduced Thermal Stabilities. Mater. Sci. Forum 722, 77–86.

Lo, S.-C.B., Heang-Ping Chan, JYyh-Shyan Lin, Huai Li, Freedman, M.T., Mun, S.K., 1995. Artificial convolution neural network for medical image pattern recognition. Neural Netw. 8, 1201–1214.

Lucas, N., Bienaime, C., Belloy, C., Queneudec, M., Silvestre, F., Nava-Saucedo, J.-E., 2008. Polymer biodegradation: Mechanisms and estimation techniques – a review. Chemosphere 73, 429–442. https://doi.org/10.1016/j.chemosphere.2008.06.064.

Luo, Lei, Li, Z., Tian, Q., Guo, Lixia, Wang, Q., 2023. Prediction of CSG splitting tensile strength based on XGBoost-RF model. Mater. Today Commun. 34, 105350 https://doi.org/10.1016/j.mtcomm.2023.105350.

Maimon, O.Z., 2010. Data mining and knowledge discovery handbook. Springer, New York.

Mallardo, S., De Vito, V., Malinconico, M., Volpe, M.G., Santagata, G., Di Lorenzo, M.L., 2016. Poly(butylene succinate)-based composites containing β-cyclodextrin/d-limonene inclusion complex. Eur. Polym. J. 79, 82–96. https://doi.org/10.1016/j.eurpolymj.2016.04.024.

Mandic, D.P., Chambers, J.A., 2001. Recurrent neural networks for prediction: learning algorithms, architectures and stability, 1st ed, Adaptive and learning systems for signal processing, communications, and control. J. Wiley, Newark.

Marom, G., 2023. Why Do Nanoparticles (CNTs) Reduce the Glass Transition Temperature of Nanocomposites. ? J. Compos. Sci. 7, 114. https://doi.org/10.3390/jcs7030114.

Marom, G., Wagner, H.D., 2020. A perspective on the structure and properties of nanocomposites. Polym. Compos. 41, 2986–2989. https://doi.org/10.1002/pc.25729.

Maulud, D., Abdulazeez, A.M., 2020. A review on linear regression comprehensive in machine learning. J. Appl. Sci. Technol. Trends 1 (2), 140–147. https://doi.org/10.38094/jastt1457.

Miller, J., Seegmiller, C., Masoum, M.A.S., Shekaramiz, M., Seibi, A.C., 2023. Hyperparameter Tuning of Support Vector Machines for Wind Turbine Detection Using Drones. 2023 Intermountain Engineering, Technology and Computing (IETC). IEEE, pp. 55–60. https://doi.org/10.1109/IETC57902.2023.10152252.

Mittal, U., Sharma, D.M., 2021. Artificial Intelligence and its Application in Different Areas of Indian Economy. Int. J. Adv. Res. Sci. Commun. Technol. 160–163. https://doi.org/10.48175/IJARSCT-V2-I3-328.

Müller,, A.J., Arnal, M.L., Trujillo, M., Lorenzo, A.T., 2011. Super-nucleation in nanocomposites and confinement effects on the crystallizable components within block copolymers, miktoarm star copolymers and nanocomposites. Eur. Polym. J. 47, 614–629.

Natarajan, B., 2022. Processing-structure-mechanical property relationships in direct formed carbon nanotube articles and their composites: A review. Compos. Sci. Technol. 225, 109501.

Nilsson, N.J., 1997. Artificial Intelligence: A New Synthesis, Artificial Intelligence: a New Synthesis. Elsevier Science & Technology, United States.

Ojijo, V., Sinha Ray, S., Sadiku, R., 2012. Role of Specific Interfacial Area in Controlling Properties of Immiscible Blends of Biodegradable Polylactide and Poly[(butylene succinate)-co-adipate. ACS Appl. Mater. Interfaces 4, 6690–6701. https://doi.org/10.1021/am301842e.

Ostertagová, E., 2012. Modelling using Polynomial Regression. Procedia Eng. 48, 500–506. https://doi.org/10.1016/j.proeng.2012.09.545.

Özkan, M., Karakoç, A., Borghei, M., Wiklund, J., Rojas, O.J., Paltakari, J., 2019. Machine Learning assisted design of tailor-made nanocellulose films: A combination of experimental and computational studies. Polym. Compos. 40, 4013–4022. https://doi.org/10.1002/pc.25262.

Patti, A., Acierno, D., 2023. Materials, Weaving Parameters, and Tensile Responses of Woven Textiles. Macromol 2023 (3), 665–680. https://doi.org/10.3390/macromol3030037.

Platnieks, O., Gaidukovs, S., Kumar Thakur, V., Barkane, A., Beluns, S., 2021. Bio-based poly (butylene succinate): Recent progress, challenges and future opportunities. Eur. Polym. J. 161, 110855 https://doi.org/10.1016/j.eurpolymj.2021.110855.

Pradeep, S.A., Kharbas, H., Turng, L.-S., Avalos, A., Lawrence, J.G., Pilla, S., 2017. Investigation of Thermal and Thermomechanical Properties of Biodegradable PLA/PBSA Composites Processed via Supercritical Fluid-Assisted Foam Injection Molding. Polymers 9, 22. https://doi.org/10.3390/polym9010022.

Qi, Z., Ye, H., Xu, J., Chen, J., Guo, B., 2013. Improved the thermal and mechanical properties of poly(butylene succinate-co-butylene adipate) by forming nanocomposites with attapulgite. Colloids Surf. A Physicochem. Eng. Asp. 421, 109–117. https://doi.org/10.1016/j.colsurfa.2012.12.051.

Qu, D., Zheng, W., Wang, B., Wu, B., Cao, H., Yi, H., 2021. Nondestructive acquisition of the micro-mechanical properties of high-speed-dry milled micro-thin walled structures based on surface traits. Chin. J. Aeronaut. 34, 438–451. https://doi.org/10.1016/j.cja.2020.08.039.

Ray, S., Haque, M., Rahman, M.M., Sakib, M.N., Al Rakib, K., 2021. Experimental investigation and SVM-based prediction of compressive and splitting tensile strength of ceramic waste aggregate concrete. J. King Saud. Univ. Eng. Sci. https://doi.org/10.1016/j.jksues.2021.08.010.

Rodrigues, M.Á.V., Horn, M.M., Martins, V.C.A., Plepis, A.M.G., 2021. Single-wall carbon nanotubes-chitosan nanocomposites: Surface wettability, mechanical and thermal properties. Mater. Werkstech. 52, 400–408. https://doi.org/10.1002/mawe.202000300.

Rosenblatt, F., 1962. Principles of neurodynamics; perceptrons and the theory of brain mechanisms. Spartan Books, Washington (State).

Sahu, S.K., Sreekanth, P.S.R., 2022. Artificial Neural Network for Prediction of Mechanical Properties of HDPE Based Nanodiamond Nanocomposite. Polym. Korea 46, 614–620. https://doi.org/10.7317/pk.2022.46.5.614.

Samir, A., Ashour, F.H., Hakim, A.A.A., et al., 2022. Recent advances in biodegradable polymers for sustainable applications. npj Mater. Degrad. 6, 68. https://doi.org/10.1038/s41529-022-00277-7.

Saxena, A., Mehta, A., Vasudev, H., Prashar, G., Yasir Jasim, N., 2023. A short review on machine learning for the Purpose of Optimizing and Predicting the Properties of Polymeric Nanocomposites. Mater. Today: Proc. https://doi.org/10.1016/j.matpr.2023.07.347.

Scerri, M., Grech, V., 2020. Artificial intelligence in medicine. Early Hum. Dev. 145, 105017 https://doi.org/10.1016/j.earlhumdev.2020.105017.

Schapire, R.E., 2003. The Boosting Approach to Machine Learning: An Overview. Nonlinear Estimation and Classification. Springer, New York, New York, NY. https://doi.org/10.1007/978-0-387-21579-2_9.

Seggiani, M., Altieri, R., Cinelli, P., Esposito, A., Lazzeri, A., 2021. Thermoplastic Blends Based on Poly(Butylene Succinate-co-Adipate) and Different Collagen Hydrolysates from Tanning Industry: I—Processing and Thermo-mechanical Properties. J. Polym. Environ. 29, 392–403. https://doi.org/10.1007/s10924-020-01880-y.

Shet, C., Chandra, N., Namilae, S., 2005. Defect-Defect Interaction in Carbon Nanotubes under Mechanical Loading. Mech. Adv. Mater. Struct. 12, 55–65. https://doi.org/10.1080/15376490490492089.

Song, Y.-Y., Ye, H.-M., Meng, X.-Y., Zhou, Q., Lu, G.-W., 2015. Novel polymorphism behavior of poly(butylene adipate) in its nanocomposites with carbon nanofibers. RSC Adv. 5, 12384–12391. https://doi.org/10.1039/c5ra19099a.

Soni, S.K., Thomas, V.R.Kar, 2020. A comprehensive review on CNTs and CNT-reinforced composites: syntheses, characteristics and applications. Mater. Today Commun. 25, 101546.

Strangis, G., Rossi, D., Cinelli, P., Seggiani, M., 2023. Seawater Biodegradable Poly (butylene succinate- co -adipate)-Wheat Bran Biocomposites. Materials 16, 2593. https://doi.org/10.3390/ma16072593.

Tasis, D., Tagmatarchis, N., Bianco, A., Prato, M., 2006. Chemistry of Carbon Nanotubes. Chem. Rev. 106, 1105–1136. https://doi.org/10.1021/cr050569o.

Tsimpliaraki, A., Svinterikos, S., Panayiotou, C., Marras, S.I., Zuburtikudis, I., Papadopoulou, L., 2010. PBSA/layered silicate nanocomposites and the role of nanoclay on their electrospun fibrous structure. Int. J. Nanomanuf. 6, 291–299. https://doi.org/10.1504/IJNM.2010.034791.

Várkonyi-Kóczy, A.R., 2020. Advances in Machine Learning Modeling Reviewing Hybrid and Ensemble Methods, Engineering for Sustainable Future. Springer International Publishing AG, Switzerland. https://doi.org/10.1007/978-3-030-36841-8_21.

Wang, G., Guo, B., Xu, J., Li, R., 2011. Rheology, crystallization behaviors, and thermal stabilities of poly(butylene succinate)/pristine multiwalled carbon nanotube composites obtained by melt compounding. J. Appl. Polym. Sci. 121, 59–67. https://doi.org/10.1002/app.33222.

Wang, Y., Zhang, M., Lin, A., Iyer, A., Prasad, A.S., Li, X., Zhang, Y., Schadler, L.S., Chen, W., Brinson, L.C., 2020. Mining structure-property relationships in polymer nanocomposites using data driven finite element analysis and multi-task convolutional neural networks. Mol. Syst. Des. Eng. 5, 962–975. https://doi.org/10.1039/d0me00020e.

Xu, J., Guo, B.-H., 2010. Poly(butylene succinate) and its copolymers: Research, development and industrialization. Biotechnol. J. 5, 1149–1163. https://doi.org/10.1002/biot.201000136.

Yang, K., Xu, X., Yang, B., Cook, B., Ramos, H., Krishnan, N.M.A., Smedskjaer, M.M., Hoover, C., Bauchy, M., 2019. Predicting the Young's Modulus of Silicate Glasses using High-Throughput Molecular Dynamics Simulations and Machine Learning. Sci. Rep. 9, 8739-11. https://doi.org/10.1038/s41598-019-45344-3.

Zakaulla, M., pasha, Y., Siddalingappa, S. kesarmadu, 2022. Prediction of mechanical properties for polyetheretherketone composite reinforced with graphene and titanium powder using artificial neural network. Mater. Today.: Proc. 49, 1268–1274. ⟨https://doi.org/10.1016/j.matpr.2021.06.365⟩.

Zamanian, M., Sadrnia, H., Khojastehpour, M., Rohani, A., Thibault, J., Hosseini, F., 2023. Multi-objective Optimization of PVA/TiO2/MMT Mixed Matrix Membrane for Food Packaging. J. Polym. Environ. 31, 90–101. https://doi.org/10.1007/s10924-022-02632-w.

Zhang, C., Zhang, Y., Shi, X., Almpanidis, G., Fan, G., Shen, X., 2019. On Incremental Learning for Gradient Boosting Decision Trees. Neural Process. Lett. 50, 957–987. https://doi.org/10.1007/s11063-019-09999-3.

Zhu, J., Wang, C., 2020. Biodegradable plastics: Green hope or greenwashing. Mar. Pollut. Bull. 161, 111774.

Zou, J., Han, Y., So, S.-S., 2008. Overview of Artificial Neural Networks. Artificial Neural Networks. Humana Press, Totowa, NJ. https://doi.org/10.1007/978-1-60327-101-1_2.